A fractional time-stepping method for unsteady thermal convection in non-Newtonian fluids

Mofdi El-Amrani[a], Anouar Obbadi[a], Mohammed Seaid[b,*], Driss Yakoubi[c]

[a]*Laboratory of Mathematics and Applications, FSTT, Abdelmalek Essaadi University, Tangier, Morocco*

[b]*Department of Engineering, University of Durham, South Road, DH1 3LE, United Kingdom*

[c]*Léonard de Vinci Pôle Universitaire, Research Center, 92 916 Paris La Défense, France*

Abstract

We propose a fractional-step method for the numerical solution of unsteady thermal convection in non-Newtonian fluids with temperature-dependent physical parameters. The proposed method is based on a viscosity-splitting approach, and it consists of four uncoupled steps where the convection and diffusion terms of both velocity and temperature solutions are uncoupled while a viscosity term is kept in the correction step at all times. This fractional-step method maintains the same boundary conditions imposed in the original problem for the corrected velocity solution, and it eliminates all inconsistencies related to boundary conditions for the treatment of the pressure solution. In addition, the method is unconditionally stable, and it allows the temperature to be transported by a non-divergence-free velocity field. In this case, we introduce a methodology to handle the subtle temperature convection term in the error analysis and establish full first-order error estimates for the velocity and the temperature solutions and $1/2$-order estimates for the pressure solution in their appropriate norms. Three numerical examples are presented to demonstrate the theoretical results and examine the performance of the proposed method for solving unsteady thermal convection in non-Newtonian fluids. The computational results obtained for the considered examples confirm the convergence, accuracy, and applicability of the proposed time fractional-step method for unsteady thermal convection in non-Newtonian fluids.

Keywords: Non-Newtonian fluids; Thermal convection; Fractional time-stepping; Viscosity-splitting method; Error analysis.

1. Introduction

Non-Newtonian fluids are characterized by a nonlinear shear stress-shear rate relationship, allowing a variety of complex flow behaviors such as blood, shampoos, fruit concentrates, coal, mineral slurries, and polymer melts, among others. In most existing rheological models including the power-law, Carreau, Carreau-Yasuda, Cross, Casson and other models, this nonlinearity is exclusively incubated in the viscosity, which becomes a function of the shear rate magnitude that multiplies the rate of deformation matrix, see for instance [31]. This class of non-Newtonian fluids maintaining the same tensorial structure as the Newtonian assumption, are also known as generalized Newtonian fluids. Based on their viscosity response to shear rate, the non-Newtonian fluids can be classified into either shear-thickening (dilatant) fluids whose viscosity increases with increasing shear rate, or shear-thinning (pseudoplastic) fluids, which are more widespread in real life and manifesting an opposite response to shear rate increase. In many industrial processes, non-Newtonian fluids are subject to the natural convection phenomenon in which the fluid is driven by the buoyancy force resulting from a vertical temperature gradient. This situation is mathematically modeled, under

*Corresponding author

Email addresses: moelamrani@uae.ac.ma (Mofdi El-Amrani), anouar.obbadi@etu.uae.ac.ma (Anouar Obbadi), m.seaid@durham.ac.uk (Mohammed Seaid), driss.yakoubi@devinci.fr (Driss Yakoubi)

the Boussinesq assumption, by a system of Navier-Stokes equations for the flow field coupled with a convection-diffusion equation for the heat distribution, see [2, 48] for more details. Here, the viscosity and thermal conductivity appearing in the system are assumed to be temperature-dependent which makes the present work physically more appealing and also more challenging. In fact, the numerical approximation of such systems presents various computational challenges. For example, the saddle point structure of the Navier-Stokes equations causes indefiniteness, and its convective term introduces nonlinearity and causes non-symmetry in the system. On the other hand, the strong velocity-temperature coupling has destabilizing effects by transporting energy from the heated side up to the cooler side (see for example [32]), and the extra nonlinearities owing to the shear rate and temperature dependency of the fluid viscosity in addition to the temperature dependency of its thermal conductivity. These features would make any three-dimensional monolithic approach very impractical, even with modern machines, since it would run into a severe algebraic system requiring highly advanced solvers and prohibitive computational resources. Therefore, a fractional-step approach is presented in the current study to alleviate this complexity in solving unsteady thermal convection in non-Newtonian fluids. Fractional-step or projection methods, based on the idea of "divide to conquer", separate the problem into two (or more) time-marching steps with less difficult sub-problems to solve in each step. These methods are attributed to the early works by Chorin [13] and Temam [51] where, the velocity and pressure are computed separately by projecting an intermediate velocity, solved in the first step, onto a solenoidal space. Although the method was shown to deliver first-order for the velocity and $1/2$-order for the pressure approximations [49], it suffered from a numerical boundary layer due to unphysical Neumann boundary conditions imposed on the pressure [52]. In the subsequent years, many attempts to overcome this drawback have delivered several relatively improved variants, such as the pressure-correction methods [24, 55, 49, 50], rotational methods [53, 25], and methods based on improved pressure boundary conditions [41, 33]. Other interesting projection methods can be found in [34, 3] and for a detailed review see for instance [26]. Recently, the extension of fractional-step methods to non-Newtonian fluid flow is gaining more attention with the efforts reported in [16, 17, 43, 42, 20] among others. Regarding natural convection problems, the fractional-step methods were jointly used with various spatial discretizations, such as finite difference and finite element methods to provide numerical simulations for the Newtonian fluids [11, 38, 40, 56, 19, 36, 57] and the non-Newtonian fluids [30, 35, 18, 9] in different computational domains and flow configurations. However, works devoted to their error analysis are far fewer even in the Newtonian case, see [45, 46, 58] for the problem with temperature-independent parameters and [15] for the problem with temperature-dependent parameters, but almost nonexistent for the non-Newtonian case.

In the present study, we are interested in the viscosity-splitting approach, which differs from the projection methods by maintaining a diffusion term in the incompressibility step, thus allowing the full original boundary conditions to be imposed and removing any physical inconsistencies related to the pressure solution. The method was introduced for incompressible flows with constant viscosity in [7] and similar ideas were earlier proposed in [39, 23, 12, 21] among others. Thereafter, error estimates were established for this method in [6] for which a first-order accuracy was demonstrated for the velocity solution, and an $1/2$-order accuracy was demonstrated for the pressure solution. Later, these estimates were improved in [27] to reach the first–order for the pressure and also in [59] for the pressure-correction version of the method. Very recently, authors in [20] extended the method to Navier-Stokes equations for the shear-thinning fluids and provided error analysis for both velocity and pressure solutions. Regarding natural convection problems, methods based on the viscosity-splitting approach have been studied only for the Newtonian fluids; see [60] for the system with temperature-independent parameters, and [29] for the problem with temperature-dependent parameters. The current work is among the first attempts to extend the viscosity-splitting approach to the shear-thinning fluids experiencing natural convection. From a physical perspective, our approach is more consistent since the viscosity coefficient which is a function of the shear rate is mainly controlled by a generic law with adjusted parameters which accordingly covers a wide range of non-Newtonian fluid regimes. Furthermore, both the viscosity and heat conductivity are allowed to be temperature-dependent in this study, and natural boundary conditions on the temperature are activated on a part of the boundary while non-homogeneous Dirichlet boundary conditions are prescribed on the other part. From a numerical perspective, the method is unconditionally stable with no concerns about numerical boundary layers since the original boundary conditions are fully preserved. Moreover, the temperature is transported here by a non-divergence-free velocity field which is to our knowledge not addressed in literature for unsteady thermal convection in non-Newtonian fluids. In the present work, the fractional time-stepping method originally proposed for solving Newtonian flow problems is extended to generalized fluids with generic rheological laws. We also perform a rigorous analysis of convergence for the proposed method and establish first-order error estimates

for both velocity and temperature solutions and $1/2$-error estimates for the pressure solution in their relevant norms. To assess the accuracy of the proposed method, we first present numerical results for a three-dimensional problem with known analytical solutions to quantify the errors. Then, we present numerical simulations for the two-dimensional benchmark problem of thermal flows past a circular cylinder with nonlinear fluid viscosity and thermal conductivity coefficients depending on the velocity and temperature solutions. The method is also applied for solving natural convection of power-law fluids in a square enclosure with differentially heated side walls. The obtained numerical results for different flow regimes confirm our theoretical expectations and illustrate good computational accuracy and stability.

The remainder of this paper is structured as follows: In section 2, we formulate the governing equations for unsteady thermal convection in non-Newtonian fluids, along with notations and preliminaries to be used in the sequel of this work. Based on some regularity assumptions on the continuous solution, the proposed fractional time-stepping method is formulated in section 3 for the variational form. In section 4, the analysis and error estimates are established for all the solutions in their relevant norms. Three numerical examples, including the problem of thermal flow past a circular cylinder, are presented in section 5 to verify the theoretical results and validate the method. Finally, section 6 contains concluding remarks.

2. Governing equations and preliminaries

In the present study, given Ω a bounded domain in $\mathbb{R}^d$ (with $d = 2$ or 3) of class $C^{1,1}$ with the boundary $\partial\Omega = \Gamma_D \cup \Gamma_N$, and $\Omega_t = \Omega \times \left(0, T_f\right)$, with $T_f > 0$ is the final time, we are interested in the numerical solution of incompressible non-Newtonian fluids undergoing a natural convection phenomenon governed by the well-established Boussinesq approximation. We assume that the fluid has a velocity $\boldsymbol{u}$, a pressure p, a temperature T and a stress tensor of the form

$$\boldsymbol{\sigma}(\boldsymbol{u}) = 2\nu \boldsymbol{Du} - p\boldsymbol{I},$$

where $\boldsymbol{I}$ is the unit matrix, $\boldsymbol{Du}$ is the shear-rate tensor defined by

$$\boldsymbol{Du} = \frac{1}{2}\left(\nabla \boldsymbol{u} + \nabla^{\top}\boldsymbol{u}\right),$$

and ν is the fluid viscosity possibly depending on the temperature and the shear-rate according to a generic law as defined below. Hence, the problem under study consists of the incompressible Navier-Stokes equations for the flow coupled with the convection-diffusion equation for the temperature as

$$\left\{\begin{array}{rcll} \dfrac{\partial \boldsymbol{u}}{\partial t} + (\boldsymbol{u}\cdot\nabla)\,\boldsymbol{u} - \nabla\cdot(2\nu(T,\boldsymbol{Du})\boldsymbol{Du}) + \nabla p &=& \boldsymbol{F}(T), & \text{in } \Omega_t, \\ \nabla\cdot\boldsymbol{u} &=& 0, & \text{in } \Omega_t, \\ \dfrac{\partial T}{\partial t} + (\boldsymbol{u}\cdot\nabla)\,T - \nabla\cdot(\lambda(T)\nabla T) &=& G, & \text{in } \Omega_t, \end{array}\right. \tag{1}$$

where λ is the thermal conductivity assumed to be dependent on the temperature, $\boldsymbol{F}$ is the external volumic force and it depends on the temperature T, and the function G represents an external heat source depending only on the position $\boldsymbol{x} \in \mathbb{R}^d$. In many practical applications in heat transfer, the function $\boldsymbol{F}$ is assumed to be proportional to the temperature difference (*i.e.* $\boldsymbol{F} \propto (T - T_0)$). Here, we allow a more general setting by assuming that $\boldsymbol{F} : \mathbb{R} \longrightarrow \mathbb{R}^d$ is a $C^1(\mathbb{R})$ function such that there exists a real T_0 and a non-negative real $\alpha > 0$ such that

$$\boldsymbol{F}(T_0) = 0, \qquad \left\|\boldsymbol{F}'\right\|_{\infty} \leq \alpha. \tag{2}$$

We also introduce the temperature $\hat{\Theta} = T - T_0$ and set the function $\boldsymbol{f}(\hat{\Theta}) = \dfrac{1}{\alpha}\boldsymbol{F}(T)$. Thus, using the above assumptions, the function $\boldsymbol{f}$ verifies

$$\boldsymbol{f}(0) = \boldsymbol{0} \qquad \text{and} \qquad \forall \ell \in \mathbb{R} \quad |\boldsymbol{f}'(\ell)| \leq 1 \implies |\boldsymbol{f}(\ell)| \leq |\ell|. \tag{3}$$

Hence, using the above change of variable, the system (1) can be expressed in terms of $\hat{\Theta}$ and $\boldsymbol{f}$ as

$$\left\{\begin{array}{rcll} \dfrac{\partial \boldsymbol{u}}{\partial t} + (\boldsymbol{u}\cdot\nabla)\,\boldsymbol{u} - \nabla\cdot(2\nu(\hat{\Theta},\boldsymbol{Du})\boldsymbol{Du}) + \nabla\, p &=& \alpha \boldsymbol{f}(\hat{\Theta}), & \text{in } \Omega_t, \\ \nabla\cdot\boldsymbol{u} &=& 0, & \text{in } \Omega_t, \\ \dfrac{\partial \hat{\Theta}}{\partial t} + (\boldsymbol{u}\cdot\nabla)\,\hat{\Theta} + \dfrac{1}{2}\hat{\Theta}\nabla\cdot\boldsymbol{u} - \nabla\cdot(\lambda(\hat{\Theta})\nabla\hat{\Theta}) &=& g, & \text{in } \Omega_t, \end{array}\right. \tag{4}$$

The system (4) is completed with the following initial conditions

$$\boldsymbol{u}(\boldsymbol{x},0) = \boldsymbol{u}^0(\boldsymbol{x}) \in \boldsymbol{L}^2(\Omega), \quad \text{with} \quad \nabla\cdot\boldsymbol{u}^0 = 0, \qquad \text{and} \qquad \hat{\Theta}(\boldsymbol{x},0) = \hat{\Theta}^0(\boldsymbol{x}) \in L^2(\Omega), \tag{5}$$

and equipped with the following boundary conditions

$$\boldsymbol{u} = 0, \ \text{ on } \partial\Omega, \qquad \hat{\Theta} = \Theta_D, \ \text{ on } \Gamma_D, \qquad \text{and} \qquad \lambda(\hat{\Theta})\frac{\partial\hat{\Theta}}{\partial \boldsymbol{n}} = \Theta_N, \ \text{ on } \Gamma_N, \qquad a.e \quad t\in(0,T_f). \tag{6}$$

Note that the viscosity ν in (4) depends on the temperature $\hat{\Theta}$ and the shear-rate tensor $\boldsymbol{Du}$. For a non-Newtonian fluid, there are several rheological laws in the literature describing the relation between the viscosity and the shear-rate, see for example [31]. Here, we consider a modified version of the Carreau law [10] in which effects of the temperature on the viscosity are not ignored, making our approach physically appealing. Therefore, the viscosity law adopted in the present work is defined by

$$\nu\left(\hat{\Theta},\boldsymbol{Du}\right) = \nu_\infty + \left(\gamma(\hat{\Theta}) - \nu_\infty\right)\left(1+\beta_0^2\,\|\boldsymbol{Du}\|^2_{\mathbb{R}^{d\times d}}\right)^{\dfrac{m-1}{2}}, \tag{7}$$

where ν_∞, β_0 and $m \le 1$ are nonnegative fixed constants characterizing the non-Newtonian fluid under study. Notice that the zeroth shear-rate viscosity γ is a function of the temperature $\hat{\Theta}$ and subsequently it incubates the temperature effects on the viscosity. In the present work, the power index m is assumed to be $m \le 1$ which corresponds to the shear-thinning behavior in non-Newtonian fluids. For simplicity in the presentation, we consider homogeneous Dirichlet boundary conditions for $\boldsymbol{u}$ and we assume that the intersection $\overline{\Gamma}_D \cap \overline{\Gamma}_N$ is a Lipschitz-continuous sub-manifold of $\partial\Omega$. We also assume that the coefficients ν and λ in (4) are bounded functions in $W^{1,\infty}(\Omega)$, with

$$\left\{\begin{array}{ll} 0 < \nu_\infty \le \nu_0 \le \gamma(s) \le \nu_1, & \|\gamma'\|_\infty = \nu_2, \\ 0 < \lambda_0 \le \lambda(s) \le \lambda_1, & \|\lambda'\|_\infty = \lambda_2, \end{array}\right. \qquad \forall s \in \mathbb{R}. \tag{8}$$

where ν_0, ν_2, λ_0, λ_1 and λ_2 are nonnegative constants. Note that, since the power index $m \le 1$, it is easy to verify that the viscosity law (7) satisfies

$$\nu_\infty \le \nu \le \nu_1. \tag{9}$$

In what follows, $L^p(\Omega)$ represents the usual set of pth power measurable functions, and $\boldsymbol{L}^p(\Omega) = (L^p(\Omega))^3$. The scalar product defined on $L^2(\Omega)$ or $\mathbf{L}^2(\Omega)$ is denoted (without distinction) by $(\cdot,\cdot)$ or by the integral notation and its associated norm by $\|\cdot\|$. The Sobolev spaces denoted by $W^{m,p}(\Omega)$ and $\boldsymbol{W}^{m,p}(\Omega)$, with the integer $p \in [1,+\infty)$, are defined as

$$W^{m,p}(\Omega) = \left\{u \in L^p(\Omega) : \quad D^{\boldsymbol{k}}u \in L^p(\Omega), \quad \forall |\boldsymbol{k}| \le m\right\}, \qquad \boldsymbol{W}^{m,p}(\Omega) = \left(W^{m,p}(\Omega)\right)^3,$$

where $\boldsymbol{k}$ is a multi-index in $\mathbb{N}^3$. These spaces are equipped with the norm $\|\cdot\|_{m,p}$ and semi-norm $|\cdot|_{m,p}$. The spaces $W^{s,2}(\Omega)$ and $\boldsymbol{W}^{s,2}(\Omega)$, with $s \in \mathbb{R}$, are denoted respectively, by $H^s(\Omega)$ and $\boldsymbol{H}^s(\Omega)$ with the associated norms denoted by $\|\cdot\|_s$ and semi-norm by $|\cdot|_s$. Without distinction for the dimension, we denote the duality pairing between $H^1_0(\Omega)$ and its dual $H^{-1}(\Omega)$ (or between $\boldsymbol{H}^1_0(\Omega)$ and $\boldsymbol{H}^{-1}(\Omega)$) by $\langle\cdot,\cdot\rangle$. More generally, for a space V and its dual V', we denote the duality pairing by $\langle\cdot,\cdot\rangle_{V',V}$. For a fixed positive real variable T_f and a separable Banach space E equipped with the norm $\|\cdot\|_E$, we denote by $C^0(0,T_f;E)$ the space of continuous functions from $[0,T_f]$ with values in E. For a positive integer p, we introduce the following Bochner spaces

$$L^p(0,T_f;E) = \left\{u : (0,T_f) \mapsto E : \qquad \left(\int_0^{T_f} \|u(\tau)\|_E^p\, d\tau\right)^{1/p} < \infty\right\},$$

and for m a non-negative integer, the space $H^m(0,T_f;E)$ is defined as

$$H^m(0,T_f;E)=\Big\{u\in L^2(0,T_f;E):\qquad \partial_t^l u\in L^2(0,T_f;E),\quad 0\le l\le m\Big\}.$$

For details on these spaces, we refer for example to [1] and [8, Chapter 2]. In order to derive the variational formulation of the problem (4), (5) and (6), we start by introducing the following spaces

$$\begin{aligned}\boldsymbol{H} &= \Big\{\boldsymbol{v}\in\boldsymbol{L}^2(\Omega):\quad \nabla\cdot\boldsymbol{v}=0,\quad \boldsymbol{v}\cdot\boldsymbol{n}\Big|_{\partial\Omega}=0\Big\},\\ \boldsymbol{V} &= \Big\{\boldsymbol{v}\in\boldsymbol{H}_0^1(\Omega):\qquad \nabla\cdot\boldsymbol{v}=0\Big\}.\end{aligned}$$

Note that the set $\boldsymbol{H}$ is the closure of $\boldsymbol{V}$ in $\boldsymbol{L}^2(\Omega)$ with $\boldsymbol{V}\subset\boldsymbol{H}\subset\boldsymbol{V}'$. We also define the temperature space as follows

$$H^1_{\Gamma_D}(\Omega)=\Big\{\varphi\in H^1(\Omega):\qquad \varphi=0,\quad \text{on}\quad \Gamma_D\Big\}.$$

The space $H^1_{\Gamma_D}(\Omega)$ can be provided with the $H^1_0(\Omega)$-norm, and based on the Poincaré-Friedrichs inequality $|\varphi|_{1,\Omega}=\|\nabla\varphi\|$. The dual of $H^1_{\Gamma_D}(\Omega)$ is denoted by $H^{-1}_{\Gamma_D}$ and its norm is also denoted by $\|\cdot\|_{-1}$ when there is no confusion and the context is clear. The traces of functions in $H^1_{\Gamma_D}(\Omega)$ on Γ_N belong to a special space $H^{\frac{1}{2}}_{00}(\Gamma_N)$, see [37, Chap.1] for the definition of this space. We also introduce its dual space $H^{\frac{1}{2}}_{00}(\Gamma_N)'$ and denote by $\langle\cdot,\cdot\rangle_{\Gamma_N}$ the duality pairing between $H^{\frac{1}{2}}_{00}(\Gamma_N)$ and $H^{\frac{1}{2}}_{00}(\Gamma_N)'$. Thus, we assume that the partition of $\partial\Omega$ into Γ_N and Γ_D is sufficiently smooth for $\mathcal{D}(\Omega\cup\Gamma_N)$ to be dense in $H^1_{\Gamma_D}(\Omega)$, and sufficient conditions for this are given in [4] among others. We also recall the following properties that can be found for example in [14]: For all $\boldsymbol{u}\in\boldsymbol{V}$, $\boldsymbol{v},\boldsymbol{w}\in\boldsymbol{H}^1(\Omega)$ and $\varphi,\psi\in H^1(\Omega)$,

$$\begin{aligned}&\int_\Omega(\boldsymbol{u}\cdot\nabla)\boldsymbol{v}\cdot\boldsymbol{v}\,d\boldsymbol{x}=0, && \int_\Omega(\boldsymbol{u}\cdot\nabla)\boldsymbol{v}\cdot\boldsymbol{w}\,d\boldsymbol{x}=-\int_\Omega(\boldsymbol{u}\cdot\nabla)\boldsymbol{w}\cdot\boldsymbol{v}\,d\boldsymbol{x},\\ &\int_\Omega(\boldsymbol{u}\cdot\nabla)\varphi\cdot\varphi\,d\boldsymbol{x}=0, && \int_\Omega(\boldsymbol{u}\cdot\nabla)\varphi\cdot\psi\,d\boldsymbol{x}=-\int_\Omega(\boldsymbol{u}\cdot\nabla)\psi\cdot\varphi\,d\boldsymbol{x},\end{aligned}\tag{10}$$

and

$$\int_\Omega(\boldsymbol{u}\cdot\nabla)\boldsymbol{v}\cdot\boldsymbol{w}\,d\boldsymbol{x}\le\begin{cases}C|\boldsymbol{u}|_1|\boldsymbol{v}|_1|\boldsymbol{w}|_1, & \text{for all } \boldsymbol{u},\boldsymbol{v},\boldsymbol{w}\in\boldsymbol{H}_0^1(\Omega),\\ C\|\boldsymbol{u}\|\,\|\boldsymbol{v}\|_2\,|\boldsymbol{w}|_1, & \text{for all } \boldsymbol{v}\in\boldsymbol{H}^2(\Omega)\cap\boldsymbol{H}_0^1(\Omega),\ \boldsymbol{u},\boldsymbol{w}\in\boldsymbol{H}_0^1(\Omega),\\ C\|\boldsymbol{u}\|\,|\boldsymbol{v}|_1\,\|\boldsymbol{w}\|_2, & \text{for all } \boldsymbol{w}\in\boldsymbol{H}^2(\Omega)\cap\boldsymbol{H}_0^1(\Omega),\ \boldsymbol{u},\boldsymbol{v}\in\boldsymbol{H}_0^1(\Omega),\\ C\|\boldsymbol{u}\|_2\,|\boldsymbol{v}|_1\,\|\boldsymbol{w}\|, & \text{for all } \boldsymbol{u}\in\boldsymbol{H}^2(\Omega)\cap\boldsymbol{H}_0^1(\Omega),\ \boldsymbol{v},\boldsymbol{w}\in\boldsymbol{H}_0^1(\Omega),\\ C|\boldsymbol{u}|_1\,|\boldsymbol{v}|_1\,\|\boldsymbol{w}\|^{1/2}\,|\boldsymbol{w}|_1^{1/2}, & \text{for all } \boldsymbol{u},\boldsymbol{v},\boldsymbol{w}\in\boldsymbol{H}_0^1(\Omega),\\ C\|\boldsymbol{u}\|^{1/2}\,|\boldsymbol{u}|_1^{1/2}\,|\boldsymbol{v}|_1\,|\boldsymbol{w}|_1, & \text{for all } \boldsymbol{u},\boldsymbol{v},\boldsymbol{w}\in\boldsymbol{H}_0^1(\Omega),\end{cases}\tag{11}$$

where C is a generic constant independent of the time step that may have different expressions at each occurrence.

3. Fractional time-stepping method for thermal convection in non-Newtonian fluids

To formulate the proposed fractional time-stepping method, we first rewrite the continuous problem (4)-(5) in a variational formulation. To this end we assume that

$$\begin{aligned}g\in L^2\left(0,T_f;L^2(\Omega)\right),\qquad &\Theta_N\in L^2\left(0,T_f;H^{\frac{1}{2}}_{00}(\Gamma_N)'\right),\\ \Theta_D\in L^2\left(0,T_f;H^{\frac{1}{2}}(\Gamma_D)\right)\cap L^\infty\left(0,T_f;L^2(\Gamma_D)\right),\qquad &\partial_t\Theta_D\in L^2\left(0,T_f;L^2(\Gamma_D)\right).\end{aligned}\tag{12}$$

Notice that the assumption $\Theta_D \in L^2(0,T_f;H^{\frac{1}{2}}(\Gamma_D))$ guarantees, thanks to Lemma 2.8 in [5], that for all $\varepsilon > 0$, there exists a lifting $\mathcal{R}_\Theta \in H^1(\Omega)$ of the value of Θ_D on Γ_D satisfying for *a.e* $t \in (0,T_f)$

$$\|\mathcal{R}_\Theta\|_{L^4(\Omega)} \leq \varepsilon \|\Theta_D\|_{H^{\frac{1}{2}}(\Gamma_D)} \qquad \text{and} \qquad \|\mathcal{R}_\Theta\|_{H^1(\Omega)} \leq c_{\mathcal{R}} \|\Theta_D\|_{H^{\frac{1}{2}}(\Gamma_D)}, \tag{13}$$

where the constant $c_{\mathcal{R}}$ depends only on the domain Ω whereas, the assumption $\partial_t \Theta_D \in L^2\left(0,T_f;L^2(\Gamma_D)\right)$ implies that $\partial_t \mathcal{R}_\Theta \in L^2\left(0,T_f;L^2(\Omega)\right)$. Hence, setting $\Theta := \hat{\Theta} - \mathcal{R}_\Theta$, a variational formulation for the system (4)-(5) is given by: Find $\boldsymbol{u} \in L^2\left(0,T_f;\boldsymbol{H}^1_0(\Omega)\right) \cap H^1\left(0,T_f;\boldsymbol{L}^2(\Omega)\right)$, $p \in L^2\left(0,T_f;L^2_0(\Omega)\right)$ and $\Theta \in L^2\left(0,T_f;H^1_{\Gamma_D}(\Omega)\right) \cap H^1\left(0,T_f;L^2(\Omega)\right)$ such that for all $(\boldsymbol{v},q,\varphi)$ in $\boldsymbol{H}^1_0(\Omega) \times L^2_0(\Omega) \times H^1_{\Gamma_D}(\Omega)$

$$\begin{aligned} \int_\Omega (\partial_t \boldsymbol{u} + (\boldsymbol{u}\cdot\nabla)\boldsymbol{u})\cdot \boldsymbol{v}\, d\boldsymbol{x} + \int_\Omega 2\nu\,(\Theta + \mathcal{R}_\Theta, \boldsymbol{Du})\ \boldsymbol{Du} : \boldsymbol{Dv}\, d\boldsymbol{x} - \int_\Omega \nabla\cdot\boldsymbol{v}\, p\, d\boldsymbol{x} &= \alpha \int_\Omega \boldsymbol{f}(\Theta+\mathcal{R}_\Theta)\cdot\boldsymbol{v}\, d\boldsymbol{x}, \\ \int_\Omega \nabla\cdot\boldsymbol{u}\, q\, d\boldsymbol{x} &= 0. \end{aligned} \tag{14}$$

$$\begin{aligned} \int_\Omega (\partial_t\Theta + \boldsymbol{u}\cdot\nabla\Theta)\ \varphi\, d\boldsymbol{x} + \int_\Omega \lambda\,(\Theta+\mathcal{R}_\Theta)\ \nabla\Theta\cdot\nabla\varphi\, d\boldsymbol{x} = \int_\Omega (-\partial_t\mathcal{R}_\Theta - \boldsymbol{u}\cdot\nabla\mathcal{R}_\Theta)\ \varphi\, d\boldsymbol{x} - \\ \int_\Omega \lambda\,(\Theta+\mathcal{R}_\Theta)\,\nabla\mathcal{R}_\Theta\cdot\nabla\varphi\, d\boldsymbol{x} + \int_\Omega g\,\varphi\, d\boldsymbol{x} + \langle\Theta_N,\varphi\rangle_{\Gamma_N}. \end{aligned} \tag{15}$$

In order to discretize the system (14)-(15) with respect to the time variable, we subdivide the time interval $[0,T_f]$ into a uniform partition of subintervals $[t_k,t_{k+1}]$, $k=0,\ldots,N$ of length $\Delta t = \dfrac{T_f}{N}$, and we denote by ω^n the approximation of any function $\omega(\boldsymbol{x},t)$ at $t=t_n$. Thus, applied to the system (4)-(5), the time splitting method proposed in the present work is carried out by the following four steps:

Step 1: Given $\boldsymbol{u}^n$, compute $\overline{\boldsymbol{u}}^{n+1}$ solution of

$$\frac{\overline{\boldsymbol{u}}^{n+1}-\boldsymbol{u}^n}{\Delta t} + (\boldsymbol{u}^n\cdot\nabla)\overline{\boldsymbol{u}}^{n+1} - \nabla\cdot\left(2\nu\left(\Theta^n+\mathcal{R}^{n+1}_\Theta,\boldsymbol{Du}^n\right)\boldsymbol{D}\overline{\boldsymbol{u}}^{n+1}\right) = \alpha\boldsymbol{f}(\Theta^n+\mathcal{R}^{n+1}_\Theta). \tag{16}$$

Step 2: Given Θ^n and $\overline{\boldsymbol{u}}^{n+1}$, compute $\overline{\Theta}^{n+1}$ solution of

$$\begin{aligned} \frac{\overline{\Theta}^{n+1}-\Theta^n}{\Delta t} + \overline{\boldsymbol{u}}^{n+1}\cdot\nabla\overline{\Theta}^{n+1} + \frac{1}{2}\overline{\Theta}^{n+1}\,\nabla\cdot\overline{\boldsymbol{u}}^{n+1} - \nabla\cdot\left(\lambda\left(\Theta^n+\mathcal{R}^{n+1}_\Theta\right)\nabla\overline{\Theta}^{n+1}\right) = \\ \nabla\cdot\left(\lambda\left(\Theta^n+\mathcal{R}^{n+1}_\Theta\right)\nabla\mathcal{R}^{n+1}_\Theta\right) - \overline{\boldsymbol{u}}^{n+1}\cdot\nabla\mathcal{R}^{n+1}_\Theta - \frac{1}{2}\mathcal{R}^{n+1}_\Theta\,\nabla\cdot\overline{\boldsymbol{u}}^{n+1} + g^{n+1} - \partial_t\mathcal{R}^{n+1}_\Theta. \end{aligned} \tag{17}$$

Step 3: Given $\boldsymbol{u}^n$, $\overline{\boldsymbol{u}}^{n+1}$ and $\overline{\Theta}^{n+1}$, compute $\left(\boldsymbol{u}^{n+1},p^{n+1}\right)$ solution of the Stokes problem

$$\begin{aligned} \frac{\boldsymbol{u}^{n+1}-\overline{\boldsymbol{u}}^{n+1}}{\Delta t} - \nabla\cdot\left(2\nu\left(\overline{\Theta}^{n+1}+\mathcal{R}^{n+1}_\Theta,\boldsymbol{Du}^n\right)\boldsymbol{Du}^{n+1}\right) + \nabla p^{n+1} &= -\nabla\cdot\left(2\nu\left(\Theta^n+\mathcal{R}^{n+1}_\Theta,\boldsymbol{Du}^n\right)\boldsymbol{D}\overline{\boldsymbol{u}}^{n+1}\right), \\ \nabla\cdot\boldsymbol{u}^{n+1} &= 0. \end{aligned} \tag{18}$$

Step 4: Given $\overline{\Theta}^{n+1}$, compute Θ^{n+1} solution of

$$\frac{\Theta^{n+1}-\overline{\Theta}^{n+1}}{\Delta t} - \nabla\cdot\left(\lambda\left(\overline{\Theta}^{n+1}+\mathcal{R}^{n+1}_\Theta\right)\nabla\Theta^{n+1}\right) = -\nabla\cdot\left(\lambda\left(\Theta^n+\mathcal{R}^{n+1}_\Theta\right)\nabla\overline{\Theta}^{n+1}\right). \tag{19}$$

Hence, the corresponding weak formulation of (16)-(19) can be obtained as follows:

Step 1: For all $\boldsymbol{v} \in \boldsymbol{H}_0^1(\Omega)$, compute $\overline{\boldsymbol{u}}^{n+1} \in \boldsymbol{H}_0^1(\Omega)$ solution of

$$\int_\Omega \frac{\overline{\boldsymbol{u}}^{n+1} - \boldsymbol{u}^n}{\Delta t} \cdot \boldsymbol{v}\, d\boldsymbol{x} + \int_\Omega (\boldsymbol{u}^n \cdot \nabla)\overline{\boldsymbol{u}}^{n+1} \cdot \boldsymbol{v}\, d\boldsymbol{x} + \int_\Omega 2\nu(\Theta^n + \mathcal{R}_\Theta^{n+1}, \boldsymbol{D}\boldsymbol{u}^n)\boldsymbol{D}\overline{\boldsymbol{u}}^{n+1} : \boldsymbol{D}\boldsymbol{v}\, d\boldsymbol{x} = \alpha \int_\Omega \boldsymbol{f}(\Theta^n + \mathcal{R}_\Theta^{n+1}) \cdot \boldsymbol{v}\, d\boldsymbol{x}. \tag{20}$$

Step 2: For all $\varphi \in H^1_{\Gamma_D}(\Omega)$, compute $\overline{\Theta}^{n+1} \in H^1_{\Gamma_D}(\Omega)$ solution of

$$\begin{aligned}\int_\Omega \frac{\overline{\Theta}^{n+1} - \Theta^n}{\Delta t}\varphi\, d\boldsymbol{x} + \int_\Omega \overline{\boldsymbol{u}}^{n+1} \cdot \nabla\overline{\Theta}^{n+1}\varphi\, d\boldsymbol{x} + \int_\Omega \frac{1}{2}\overline{\Theta}^{n+1}\nabla \cdot \overline{\boldsymbol{u}}^{n+1}\varphi\, d\boldsymbol{x} + \\ \int_\Omega \lambda(\Theta^n + \mathcal{R}_\Theta^{n+1})\nabla\overline{\Theta}^{n+1} \cdot \nabla\varphi\, d\boldsymbol{x} = -\int_\Omega \lambda(\Theta^n + \mathcal{R}_\Theta^{n+1})\nabla\mathcal{R}_\Theta^{n+1}\nabla\varphi\, d\boldsymbol{x} - \int_\Omega \overline{\boldsymbol{u}}^{n+1} \cdot \nabla\mathcal{R}_\Theta^{n+1}\varphi\, d\boldsymbol{x} - \\ \int_\Omega \frac{1}{2}\mathcal{R}_\Theta^{n+1}\nabla \cdot \overline{\boldsymbol{u}}^{n+1}\varphi\, d\boldsymbol{x} + \int_\Omega g^{n+1}\varphi\, d\boldsymbol{x} + \langle \Theta_N^{n+1}, \varphi\rangle - \int_\Omega \partial_t\mathcal{R}_\Theta^{n+1}\varphi\, d\boldsymbol{x}.\end{aligned} \tag{21}$$

Step 3: For all $(\boldsymbol{v}, q) \in \boldsymbol{V} \times L_0^2(\Omega)$, compute $\left(\boldsymbol{u}^{n+1}, p^{n+1}\right) \in \boldsymbol{V} \times L_0^2(\Omega)$ solution of the following Stokes problem

$$\begin{aligned}\int_\Omega \frac{\boldsymbol{u}^{n+1} - \overline{\boldsymbol{u}}^{n+1}}{\Delta t} \cdot \boldsymbol{v}\, d\boldsymbol{x} + \int_\Omega 2\nu(\overline{\Theta}^{n+1} + \mathcal{R}_\Theta^{n+1}, \boldsymbol{D}\boldsymbol{u}^n)\boldsymbol{D}\boldsymbol{u}^{n+1} : \boldsymbol{D}\boldsymbol{v}\, d\boldsymbol{x} - \int_\Omega p^{n+1}\nabla \cdot \boldsymbol{v}\, d\boldsymbol{x} \\ = \int_\Omega 2\nu(\Theta^n + \mathcal{R}_\Theta^{n+1}, \boldsymbol{D}\boldsymbol{u}^n)\boldsymbol{D}\overline{\boldsymbol{u}}^{n+1} : \boldsymbol{D}\boldsymbol{v}\, d\boldsymbol{x}, \\ -\int_\Omega q\nabla \cdot \boldsymbol{u}^{n+1}\, d\boldsymbol{x} = 0.\end{aligned} \tag{22}$$

Step 4: For all $\varphi \in H^1_{\Gamma_D}(\Omega)$, compute $\Theta^{n+1} \in H^1_{\Gamma_D}(\Omega)$ solution of

$$\int_\Omega \frac{\Theta^{n+1} - \overline{\Theta}^{n+1}}{\Delta t}\varphi\, d\boldsymbol{x} + \int_\Omega \lambda\left(\overline{\Theta}^{n+1} + \mathcal{R}_\Theta^{n+1}\right)\nabla\Theta^{n+1} \cdot \nabla\varphi\, d\boldsymbol{x} = \int_\Omega \lambda\left(\Theta^n + \mathcal{R}_\Theta^{n+1}\right)\nabla\overline{\Theta}^{n+1} \cdot \nabla\varphi\, d\boldsymbol{x}. \tag{23}$$

It should be noted that the well-posedness of each step in the proposed scheme can be easily verified using the assumptions (8), (12), (13) along with the usual arguments of steady linear elliptic problems for the steps (20), (21), (23) and the arguments of steady Stokes problem for the step (22), see [22] for more details. This yields the following results:

Lemma 1. *Assume $2\nu_\infty > \nu_1$ and $2\lambda_0 > \lambda_1$ and for large enough ν_∞ and λ_0, the approximate velocities $\boldsymbol{u}^{n+1}$, $\overline{\boldsymbol{u}}^{n+1}$ and temperatures Θ^{n+1}, $\overline{\Theta}^{n+1}$ verify*

$$\begin{aligned}&\|\boldsymbol{u}^{N+1}\|^2 + \|\Theta^{N+1}\|^2 + \sum_{n=0}^{N}\left(\|\boldsymbol{u}^{n+1} - \bar{\boldsymbol{u}}^{n+1}\|^2 + \|\bar{\boldsymbol{u}}^{n+1} - \boldsymbol{u}^n\|^2 + \|\Theta^{n+1} - \bar{\Theta}^{n+1}\|^2 + \|\bar{\Theta}^{n+1} - \Theta^n\|^2\right) + \\ &2C_r\Delta t\sum_{n=0}^{N}\left(\frac{\nu_\infty}{4}|\bar{\boldsymbol{u}}^{n+1}|_1^2 + (2\nu_\infty - \nu_1)|\boldsymbol{u}^{n+1}|_1^2 + \nu_\infty|\boldsymbol{u}^{n+1} - \bar{\boldsymbol{u}}^{n+1}|_1^2\right) + \Delta t\sum_{n=0}^{N}\left(\frac{\lambda_0}{2}|\bar{\Theta}^{n+1}|_1^2 + (2\lambda_0 - \lambda_1)|\Theta^{n+1}|_1^2 + \lambda_0|\Theta^{n+1} - \bar{\Theta}^{n+1}|_1^2\right) \\ &\qquad \le \|\boldsymbol{u}_0\|^2 + \|\Theta_0\|^2 + \Delta t(2\lambda_0 - \lambda_1)|\Theta_0|_1^2 + C\left(\|\partial_t\Theta_D\|^2_{L^2(0,T_f;L^2(\Gamma_D))} + \|g\|^2_{L^2(0,T_f;L^2(\Omega))} + \|\Theta_N\|^2_{L^2\left(0,T_f;H^{\frac{1}{2}}_{00}(\Gamma_N)'\right)}\right).\end{aligned}$$

We also announce the following discrete Gronwall lemma [28] that will be used several times in what follows:

Lemma 2. *For $n \in \mathbb{N}$, let κ, a_n, b_n, c_n and d_n be nonnegative numbers such that*

$$a_N + \Delta t \sum_{n=0}^{N} b_n \leq \kappa + \Delta t \sum_{n=0}^{N-1} a_n\, d_n + \Delta t \sum_{n=0}^{N-1} c_n, \qquad \forall\ N \geq 1.$$

Then, for all $N \geq 1$, the following inequality

$$a_N + \Delta t \sum_{n=0}^{N} b_n \leq \left(\kappa + \Delta t \sum_{n=0}^{N-1} c_n\right) \exp\left(\Delta t \sum_{n=0}^{N-1} d_n\right),$$

holds.

For the purpose of analysis, we also use the algebraic identity

$$2(a-b)a = a^2 - b^2 + (a-b)^2, \tag{24}$$

where a and b are nonnegative generic numbers. In addition, we introduce the notation $\overline{e}_{\Theta}^{n+1}$, e_{Θ}^{n+1}, $\overline{\boldsymbol{e}}_{u}^{n+1}$ and $\boldsymbol{e}_{u}^{n+1}$ to denote respectively, the semi-discrete errors associated to $\overline{\Theta}^{n+1}$, Θ^{n+1}, $\overline{\boldsymbol{u}}^{n+1}$ and $\boldsymbol{u}^{n+1}$ defined as

$$\begin{aligned} \overline{e}_{\Theta}^{n+1} &= \Theta(t_{n+1}) - \overline{\Theta}^{n+1}, \qquad & e_{\Theta}^{n+1} &= \Theta(t_{n+1}) - \Theta^{n+1}, \\ \overline{\boldsymbol{e}}_{u}^{n+1} &= \boldsymbol{u}(t_{n+1}) - \overline{\boldsymbol{u}}^{n+1}, \qquad & \boldsymbol{e}_{u}^{n+1} &= \boldsymbol{u}(t_{n+1}) - \boldsymbol{u}^{n+1}. \end{aligned}$$

Note that to simplify notations in the forthcoming proofs, we also denote $\Theta_{\mathcal{R}}(t_{n+1}) = \Theta(t_{n+1}) + \mathcal{R}_{\Theta}(t_{n+1})$, $\Theta_{\mathcal{R}}^{n} = \Theta^{n} + \mathcal{R}_{\Theta}^{n+1}$ and $\overline{\Theta}_{\mathcal{R}}^{n+1} = \overline{\Theta}^{n+1} + \mathcal{R}_{\Theta}^{n+1}$.

4. Error estimates for the fractional time-stepping method

In this section we first establish the error estimates in $l^{\infty}(0,T;\boldsymbol{L}^2(\Omega))$ and $l^2(0,T;\boldsymbol{H}^1(\Omega))$ norms for the approximation of $\boldsymbol{u}$ by the semi-discrete velocities $\overline{\boldsymbol{u}}^{n+1}$ and $\boldsymbol{u}^{n+1}$ using (20) in Step 2 and (22) in Step 4, which give a bound where some terms still appear in the temperature solution. Next, this bound is injected into the temperature error bound, which is established later using (21) in Step 1 and (23) in Step 3 to obtain 1/2-order estimates for the approximation of Θ by the semi-discrete temperature solutions $\overline{\Theta}^{n+1}$ and Θ^{n+1} in $l^{\infty}(0,T,L^2(\Omega))$ and $l^2(0,T;H^1(\Omega))$ norms. Therefore, injecting these last temperature estimates back into the velocity error bound would ensure 1/2-order estimates for the semi-discrete velocity solutions as well. Finally, these bounds are improved to reach the full first-order estimates for both velocity and the temperature solutions. We also provide error estimates for the pressure approximation using the considered fractional time-stepping method. To this end, let us set the following assumptions which will be repeatedly used in proofs of the error estimates established in this section

$$\begin{cases} \displaystyle\sup_{t\in(0,T_f)} \left\{\|\Theta(t)\|_2^2 + \|\partial_{tt}\Theta\|_{-1}^2 + \|\partial_t\Theta\|^2\right\} \leq C, & (25) \\ \displaystyle\sup_{t\in(0,T_f)} \left\{\|\boldsymbol{u}\|_2^2 + \|\partial_{tt}\boldsymbol{u}\|_{-1}^2 + \|\partial_t\boldsymbol{u}\|^2 + \|p(t)\|_1^2\right\} \leq C, & (26) \\ \boldsymbol{u} \in L^{\infty}\left(0,T_f;\boldsymbol{W}^{2,3+s}(\Omega)\right),\ s>0, \quad \text{which implies} \quad \displaystyle\sup_{t\in(0,T_f)} \|\nabla\boldsymbol{u}(t)\|_{\mathbf{R}^{d\times d}}^2 \leq C, & (27) \\ \Theta \in L^{\infty}\left(0,T_f;W^{2,3+s}(\Omega)\right),\ s>0, \quad \text{which implies} \quad \displaystyle\sup_{t\in(0,T_f)} \|\nabla\Theta(t)\|_{\mathbf{R}^d}^2 \leq C, & (28) \end{cases}$$

where C is a generic constant independent of Δt which may have different expressions at each occurrence. The following lemma delivers a first bound for the velocity errors $\overline{\boldsymbol{e}}_{u}^{n+1}$ and $\boldsymbol{e}_{u}^{n+1}$ in $Ł^{\infty}(0,T;\boldsymbol{L}^2(\Omega))$ and $L^2(0,T;\boldsymbol{H}^1(\Omega))$ norms:

Lemma 3. *Assuming* $\nu_1 \leq 2\nu_\infty$ *and*

$$\frac{40\, C_u^2\, C_\nu^2}{\nu_\infty C_r} \leq C_r \frac{2\nu_\infty - \nu_1}{4}, \tag{29}$$

then

$$\|\boldsymbol{e}_u^{N+1}\|^2 + \sum_{n=0}^{N}\left(\|\overline{\boldsymbol{e}}_u^{n+1} - \boldsymbol{e}_u^n\|^2 + \frac{1}{2}\|\boldsymbol{e}_u^{n+1} - \overline{\boldsymbol{e}}_u^{n+1}\|^2\right) + C_r\,\Delta t \sum_{n=0}^{N}\left(\nu_\infty|\overline{\boldsymbol{e}}_u^{n+1}|_1^2 + (2\nu_\infty - \nu_1)|\boldsymbol{e}_u^{n+1}|_1^2 + \nu_\infty|\boldsymbol{e}_u^{n+1} - \overline{\boldsymbol{e}}_u^{n+1}|_1^2\right)$$
$$\leq C\Delta t + C\Delta t \sum_{n=0}^{N}\left(\|e_\Theta^n\|^2 + \|\overline{e}_\Theta^{n+1} - e_\Theta^n\|^2\right). \tag{30}$$

Proof. Writing the first equation of (14) at $t = t_{n+1}$ using Taylor expansion with integral remainder, subtracting (20) from the result and choosing $\boldsymbol{v} = 2\Delta t\overline{\boldsymbol{e}}^{n+1}$, we obtain

$$\int_\Omega\left(\frac{\boldsymbol{u}(t_{n+1}) - \boldsymbol{u}(t_n)}{\Delta t} + (\boldsymbol{u}(t_{n+1})\cdot\nabla)\boldsymbol{u}(t_{n+1})\right)\cdot\boldsymbol{v}\; d\boldsymbol{x} + \int_\Omega 2\nu(\Theta_{\mathcal{R}}(t_{n+1}), \boldsymbol{Du}(t_{n+1}))\,\boldsymbol{Du}(t_{n+1}) : \boldsymbol{Dv}\; d\boldsymbol{x} - \int_\Omega \nabla\cdot\boldsymbol{v}\; p\; d\boldsymbol{x}$$
$$= \alpha\int_\Omega \boldsymbol{f}(\Theta_{\mathcal{R}}(t_{n+1}))\cdot\boldsymbol{v}\; d\boldsymbol{x} + \langle\boldsymbol{I}_u^n, \boldsymbol{v}\rangle, \tag{31}$$

where $\boldsymbol{I}_u^n$ is the truncation error associated to the velocity $\boldsymbol{u}$ and defined as

$$\boldsymbol{I}_u^n = \frac{1}{\Delta t}\int_{t_n}^{t_{n+1}} (t - t_n)\partial_{tt}\boldsymbol{u}(t)dt.$$

Substracting (20) from (31), choosing $\boldsymbol{v} = 2\Delta t\overline{\boldsymbol{e}}_u^{n+1}$ and using the algebraic identity (24), we have

$$\begin{aligned}
&\|\overline{\boldsymbol{e}}_u^{n+1}\|^2 - \|\boldsymbol{e}_u^n\|^2 + \|\overline{\boldsymbol{e}}_u^{n+1} - \boldsymbol{e}_u^n\|^2 + 4\Delta t\int_\omega \nu(\Theta_{\mathcal{R}}^n, \boldsymbol{Du}^n)\,\boldsymbol{D}\overline{\boldsymbol{e}}^{n+1} : \boldsymbol{D}\overline{\boldsymbol{e}}^{n+1}\; d\boldsymbol{x}\\
&\quad = 2\alpha\Delta t\int_\Omega\left(\boldsymbol{f}(\Theta_{\mathcal{R}}(t_{n+1})) - \boldsymbol{f}(\Theta_{\mathcal{R}}^n)\right)\cdot\overline{\boldsymbol{e}}_u^{n+1}\; d\boldsymbol{x} - 2\Delta t\int_\Omega \nabla p(t_{n+1})\cdot\overline{\boldsymbol{e}}_u^{n+1}\; d\boldsymbol{x}\\
&\quad - 2\Delta t\int_\Omega(\boldsymbol{u}(t_{n+1})\cdot\nabla)\boldsymbol{u}(t_{n+1})\cdot\overline{\boldsymbol{e}}_u^{n+1}\; d\boldsymbol{x} + 2\Delta t\int_\Omega(\boldsymbol{u}^n\cdot\nabla)\overline{\boldsymbol{u}}_u^{n+1}\cdot\overline{\boldsymbol{e}}_u^{n+1}\; d\boldsymbol{x} + 2\Delta t\langle\boldsymbol{I}_u^n, \overline{\boldsymbol{e}}_u^{n+1}\rangle\\
&\quad - 4\Delta t\int_\Omega\left(\nu(\Theta_{\mathcal{R}}(t_{n+1}), \boldsymbol{Du}(t_{n+1})) - \nu(\Theta_{\mathcal{R}}^n, \boldsymbol{Du}^n)\right)\boldsymbol{Du}(t_{n+1}) :\, \boldsymbol{D}\overline{\boldsymbol{e}}_u^{n+1}\; d\boldsymbol{x}.
\end{aligned} \tag{32}$$

Setting $\boldsymbol{v} = 2\Delta t\boldsymbol{e}_u^{n+1}$ in (22), we obtain

$$\begin{aligned}
&\|\boldsymbol{e}_u^{n+1}\|^2 - \|\overline{\boldsymbol{e}}_u^{n+1}\|^2 + \|\boldsymbol{e}_u^{n+1} - \overline{\boldsymbol{e}}_u^{n+1}\|^2 + 2\Delta t\int_\Omega\left(2\nu(\overline{\Theta}_{\mathcal{R}}^{n+1}, \boldsymbol{Du}^n) - \nu(\Theta_{\mathcal{R}}^n, \boldsymbol{Du}^n)\right)\boldsymbol{De}_u^{n+1} :\, \boldsymbol{De}_u^{n+1}\; d\boldsymbol{x}\\
&\quad - 2\Delta t\int_\Omega \nu(\Theta_{\mathcal{R}}^n, \boldsymbol{Du}^n)\boldsymbol{D}\overline{\boldsymbol{e}}_u^{n+1} :\, \boldsymbol{D}\overline{\boldsymbol{e}}_u^{n+1}\; d\boldsymbol{x} + 2\Delta t\int_\Omega \nu(\Theta_{\mathcal{R}}^n, \boldsymbol{Du}^n)\boldsymbol{D}(\boldsymbol{e}_u^{n+1} - \overline{\boldsymbol{e}}_u^{n+1}) :\, \boldsymbol{D}(\boldsymbol{e}_u^{n+1} - \overline{\boldsymbol{e}}_u^{n+1})\; d\boldsymbol{x}\\
&\quad = 4\Delta t\int_\Omega\left(\nu(\overline{\Theta}_{\mathcal{R}}^{n+1}, \boldsymbol{Du}^n) - \nu(\Theta_{\mathcal{R}}^n, \boldsymbol{Du}^n)\right)\boldsymbol{Du}(t_{n+1}) :\, \boldsymbol{De}_u^{n+1}\; d\boldsymbol{x}.
\end{aligned} \tag{33}$$

Adding (33) to (32), using the viscosity bounds (9) and the Korn's inequality with its constant denoted by C_r, we

obtain

$$\begin{aligned}
\|\boldsymbol{e}_u^{n+1}\|^2 - \|\boldsymbol{e}_u^{n}\|^2 + \|\overline{\boldsymbol{e}}_u^{n+1} - \boldsymbol{e}_u^{n}\|^2 + \|\boldsymbol{e}_u^{n+1} - \overline{\boldsymbol{e}}_u^{n+1}\|^2 + 2C_r\,\Delta t\left(\nu_\infty|\overline{\boldsymbol{e}}_u^{n+1}|_1^2 + (2\nu_\infty - \nu_1)|\boldsymbol{e}_u^{n+1}|_1^2 + \nu_\infty|\boldsymbol{e}_u^{n+1} - \overline{\boldsymbol{e}}_u^{n+1}|_1^2\right)\\
\leq 2\Delta t\langle \boldsymbol{I}_u^n, \overline{\boldsymbol{e}}_u^{n+1}\rangle + 2\alpha\Delta t\int_\Omega \left(\boldsymbol{f}(\Theta_{\mathcal{R}}(t_{n+1})) - \boldsymbol{f}(\Theta_{\mathcal{R}}^n)\right)\cdot\overline{\boldsymbol{e}}_u^{n+1}\,d\boldsymbol{x} - 2\Delta t\int_\Omega \nabla p(t_{n+1})\cdot\overline{\boldsymbol{e}}_u^{n+1}\,d\boldsymbol{x}\\
- 2\Delta t\int_\Omega (\boldsymbol{u}(t_{n+1})\cdot\nabla)\boldsymbol{u}(t_{n+1})\cdot\overline{\boldsymbol{e}}_u^{n+1}\,d\boldsymbol{x} + 2\Delta t\int_\Omega (\boldsymbol{u}^n\cdot\nabla)\overline{\boldsymbol{u}}_u^{n+1}\cdot\overline{\boldsymbol{e}}_u^{n+1}\,d\boldsymbol{x}\\
- 4\Delta t\int_\Omega \left(\nu(\Theta_{\mathcal{R}}(t_{n+1}), \boldsymbol{D}\boldsymbol{u}(t_{n+1})) - \nu(\Theta_{\mathcal{R}}^n, \boldsymbol{D}\boldsymbol{u}^n)\right)\boldsymbol{D}\boldsymbol{u}(t_{n+1}) :\, \boldsymbol{D}\overline{\boldsymbol{e}}_u^{n+1}\,d\boldsymbol{x}\\
+ 4\Delta t\int_\Omega \left(\nu(\overline{\Theta}_{\mathcal{R}}^{n+1}, \boldsymbol{D}\boldsymbol{u}^n) - \nu(\Theta_{\mathcal{R}}^n, \boldsymbol{D}\boldsymbol{u}^n)\right)\boldsymbol{D}\boldsymbol{u}(t_{n+1}) :\, \boldsymbol{D}\boldsymbol{e}_u^{n+1}\,d\boldsymbol{x}. \quad (34)
\end{aligned}$$

The right-hand side terms are bounded as follows

$$\begin{aligned}
2\Delta t\langle \boldsymbol{I}_u^n, \overline{\boldsymbol{e}}_u^{n+1}\rangle &\leq C\Delta t\|\boldsymbol{I}_u^n\|_{-1}^2 + \frac{C_r\,\nu_\infty\Delta t}{5}|\overline{\boldsymbol{e}}_u^{n+1}|_1^2,\\
&\leq \frac{C}{\Delta t}\|\int_{t_n}^{t_{n+1}}(t-t_n)\partial_{tt}\boldsymbol{u}(t)dt\|_{-1}^2 + \frac{C_r\,\nu_\infty\Delta t}{5}|\overline{\boldsymbol{e}}_u^{n+1}|_1^2,\\
&\leq C(\Delta t)^2\int_{t_n}^{t_{n+1}}\|\partial_{tt}\boldsymbol{u}\|_{-1}^2 dt + \frac{C_r\,\nu_\infty\Delta t}{5}|\overline{\boldsymbol{e}}_u^{n+1}|_1^2.
\end{aligned}$$

The second assumption in (3) and the Poincaré inequality on $\overline{\boldsymbol{e}}_u^{n+1}$, yield

$$\begin{aligned}
2\alpha\Delta t\int_\Omega \left(\boldsymbol{f}(\Theta_{\mathcal{R}}(t_{n+1})) - \boldsymbol{f}(\Theta_{\mathcal{R}}^n)\right)\cdot\overline{\boldsymbol{e}}_u^{n+1}\,d\boldsymbol{x} &\leq 2\alpha\Delta t\|\Theta(t_{n+1}) - \Theta(t_n) + e_\Theta^n\|\,\|\overline{\boldsymbol{e}}_u^{n+1}\|,\\
&\leq C(\Delta t)^2\int_{t_n}^{t_{n+1}}\|\partial_t\Theta\|^2 dt + C\Delta t\|e_\Theta^n\|^2 + \frac{C_r\nu_\infty\Delta t}{5}|\overline{\boldsymbol{e}}_u^{n+1}|_1^2.
\end{aligned}$$

Using the divergence-free property of $\boldsymbol{e}_u^{n+1}$, the pressure term is bounded by

$$\begin{aligned}
-2\Delta t\int_\Omega \nabla p(t_{n+1})\cdot\overline{\boldsymbol{e}}_u^{n+1}\,d\boldsymbol{x} &= 2\Delta t\int_\Omega \nabla p(t_{n+1})\cdot\left(\boldsymbol{e}_u^{n+1} - \overline{\boldsymbol{e}}_u^{n+1}\right)d\boldsymbol{x},\\
&\leq 2\Delta t|p(t_{n+1})|_1\,\|\boldsymbol{e}_u^{n+1} - \overline{\boldsymbol{e}}_u^{n+1}\|,\\
&\leq C(\Delta t)^2|p(t_{n+1})|_1^2 + \frac{1}{2}\|\boldsymbol{e}_u^{n+1} - \overline{\boldsymbol{e}}_u^{n+1}\|^2.
\end{aligned}$$

The nonlinear term can be simplified using the assumptions (10), then bounded using (11) and (26) as

$$\begin{aligned}
-2\Delta t\left(\int_\Omega (\boldsymbol{u}(t_{n+1})\cdot\nabla)\boldsymbol{u}(t_{n+1})\cdot\overline{\boldsymbol{e}}_u^{n+1}\,d\boldsymbol{x} - \int_\Omega (\boldsymbol{u}^n\cdot\nabla)\overline{\boldsymbol{u}}^{n+1}\cdot\overline{\boldsymbol{e}}_u^{n+1}\,d\boldsymbol{x}\right),\\
= -2\Delta t\left(\int_\Omega (\boldsymbol{u}(t_{n+1})\cdot\nabla)\boldsymbol{u}(t_{n+1})\cdot\overline{\boldsymbol{e}}_u^{n+1}\,d\boldsymbol{x} - \int_\Omega (\boldsymbol{u}^n\cdot\nabla)\boldsymbol{u}(t_{n+1})\cdot\overline{\boldsymbol{e}}_u^{n+1}\,d\boldsymbol{x}\right),\\
= -2\Delta t\int_\Omega ((\boldsymbol{u}(t_{n+1}) - \boldsymbol{u}(t_n))\cdot\nabla)\,\boldsymbol{u}(t_{n+1})\cdot\overline{\boldsymbol{e}}_u^{n+1}\,d\boldsymbol{x} - 2\Delta t\int_\Omega (\boldsymbol{e}_u^n\cdot\nabla)\boldsymbol{u}(t_{n+1})\cdot\overline{\boldsymbol{e}}_u^{n+1}\,d\boldsymbol{x},\\
\leq 2\Delta t\|\boldsymbol{u}(t_{n+1}) - \boldsymbol{u}(t_n)\|\,\|\boldsymbol{u}(t_{n+1})\|_2\,|\overline{\boldsymbol{e}}_u^{n+1}|_1 + 2\Delta t\|\boldsymbol{e}_u^n\|\,\|\boldsymbol{u}(t_{n+1})\|_2\,|\overline{\boldsymbol{e}}_u^{n+1}|_1,\\
\leq C(\Delta t)^2\int_{t_n}^{t_{n+1}}\|\partial_t\boldsymbol{u}\|^2 dt + C\Delta t\|\boldsymbol{e}_u^n\|^2 + \frac{C_r\nu_\infty\Delta t}{5}|\overline{\boldsymbol{e}}_u^{n+1}|_1^2,
\end{aligned}$$

The last two terms of (34) are bounded by (see Appendix A)

$$\begin{aligned}
-4\Delta t\int_\Omega \left(\nu(\Theta_{\mathcal{R}}(t_{n+1}), \boldsymbol{D}\boldsymbol{u}(t_{n+1})) - \nu(\Theta_{\mathcal{R}}^n, \boldsymbol{D}\boldsymbol{u}^n)\right)\boldsymbol{D}\boldsymbol{u}(t_{n+1}) :\, \boldsymbol{D}\overline{\boldsymbol{e}}_u^{n+1}\,d\boldsymbol{x} \leq C\Delta t\|e_\Theta^n\|^2 + \frac{40\,C_u^2\,C_\nu^2}{\nu_\infty C_r}\Delta t|\boldsymbol{e}_u^n|_1^2 +\\
C(\Delta t)^2\int_{t_n}^{t_{n+1}}\|\partial_t\Theta\|^2 dt + C(\Delta t)^2\int_{t_n}^{t_{n+1}}|\partial_t\boldsymbol{u}|_1^2 dt + 2\frac{C_r\nu_\infty\Delta t}{5}|\overline{\boldsymbol{e}}_u^{n+1}|_1^2,
\end{aligned}$$

and

$$4\Delta t \int_\Omega \Big(\nu(\overline{\Theta}_{\mathcal{R}}^{n+1}, \boldsymbol{Du}^n) - \nu(\Theta_{\mathcal{R}}^n, \boldsymbol{Du}^n)\Big)\boldsymbol{Du}(t_{n+1}) : \boldsymbol{De}_u^{n+1}\, d\boldsymbol{x} \le C\Delta t \|\overline{e}_\Theta^{n+1} - e_\Theta^n\|^2 + (2\nu_\infty - \nu_1)C_r\Delta t|\boldsymbol{e}_u^{n+1}|_1^2 + C(\Delta t)^2 \int_{t_n}^{t_{n+1}} \|\partial_t\Theta\|^2 dt.$$

Collecting all the above inequalities and considering (29), we obtain

$$\begin{aligned}\|\boldsymbol{e}_u^{n+1}\|^2 - \|\boldsymbol{e}_u^n\|^2 + \|\overline{\boldsymbol{e}}_u^{n+1} - \boldsymbol{e}_u^n\|^2 + \frac{1}{2}\|\boldsymbol{e}_u^{n+1} - \overline{\boldsymbol{e}}_u^{n+1}\|^2 + C_r\,\Delta t\left(\nu_\infty|\overline{\boldsymbol{e}}_u^{n+1}|_1^2 + (2\nu_\infty - \nu_1)|\boldsymbol{e}_u^{n+1}|_1^2 + \nu_\infty|\boldsymbol{e}_u^{n+1} - \overline{\boldsymbol{e}}_u^{n+1}|_1^2\right)\\ \le C\Delta t\left(\|e_\Theta^n\|^2 + \|\overline{e}_\Theta^{n+1} - e_\Theta^n\|^2\right) + C\Delta t\|\boldsymbol{e}_u^n\|^2 + C(\Delta t)^2\int_{t_n}^{t_{n+1}}\left(\|\partial_{tt}\boldsymbol{u}\|_{-1}^2 + \|\partial_t\Theta\|^2 + \|\partial_t\boldsymbol{u}\|^2 + |\partial_t\boldsymbol{u}|_1^2\right)dt\\ + C(\Delta t)^2|p(t_{n+1})|_1^2 + \frac{40\,C_u^2\,C_\nu^2}{\nu_\infty C_r}\Delta t|\boldsymbol{e}_u^n|_1^2.\end{aligned}$$

Taking the sum over $n = 0, 1, \ldots, N$, we get

$$\begin{aligned}\|\boldsymbol{e}_u^{N+1}\|^2 + \sum_{n=0}^{N}\left(\|\overline{\boldsymbol{e}}_u^{n+1} - \boldsymbol{e}_u^n\|^2 + \frac{1}{2}\|\boldsymbol{e}_u^{n+1} - \overline{\boldsymbol{e}}_u^{n+1}\|^2\right) + C_r\,\Delta t\sum_{n=0}^{N}\left(\nu_\infty|\overline{\boldsymbol{e}}_u^{n+1}|_1^2 + (2\nu_\infty - \nu_1)|\boldsymbol{e}_u^{n+1}|_1^2 + \nu_\infty|\boldsymbol{e}_u^{n+1} - \overline{\boldsymbol{e}}_u^{n+1}|_1^2\right)\\ \le C\Delta t\left(\|e_\Theta^n\|^2 + \|\overline{e}_\Theta^{n+1} - e_\Theta^n\|^2\right) + C\Delta t\sum_{n=0}^{N}\|\boldsymbol{e}_u^n\|^2 + C(\Delta t)^2\int_0^{T_f}\left(\left(\|\partial_{tt}\boldsymbol{u}\|_{-1}^2 + \|\partial_t\Theta\|^2 + \|\partial_t\boldsymbol{u}\|^2 + |\partial_t\boldsymbol{u}|_1^2\right)dt\right.\\ + C(\Delta t)^2\sum_{n=0}^{N}|p(t_{n+1})|_1^2 + \frac{40\,C_u^2\,C_\nu^2}{\nu_\infty C_r}\Delta t\sum_{n=0}^{N}|\boldsymbol{e}_u^n|_1^2.\end{aligned}$$

By virtue of (29), we can move the last term to the right-hand side, and using the assumptions (26), (25), the above inequality becomes

$$\begin{aligned}\|\boldsymbol{e}_u^{N+1}\|^2 + \frac{1}{2}(2\nu_\infty - \nu_1)|\boldsymbol{e}_u^{N+1}|_1^2 + \sum_{n=0}^{N}\|\overline{\boldsymbol{e}}_u^{n+1} - \boldsymbol{e}_u^n\|^2 + \frac{1}{2}\sum_{n=0}^{N}\|\boldsymbol{e}_u^{n+1} - \overline{\boldsymbol{e}}_u^{n+1}\|^2\\ + C_r\,\Delta t\sum_{n=0}^{N}\left(\nu_\infty|\overline{\boldsymbol{e}}_u^{n+1}|_1^2 + \frac{1}{2}(2\nu_\infty - \nu_1)|\boldsymbol{e}_u^{n+1}|_1^2 + \nu_\infty|\boldsymbol{e}_u^{n+1} - \overline{\boldsymbol{e}}_u^{n+1}|_1^2\right)\\ \le C\Delta t + C\Delta t\left(\|e_\Theta^n\|^2 + \|\overline{e}_\Theta^{n+1} - e_\Theta^n\|^2\right) + C\Delta t\sum_{n=0}^{N}\|\boldsymbol{e}_u^n\|^2.\end{aligned}$$

Applying the Gronwall lemma (2) ends the proof.

■

In order to establish the temperature error estimates announced in the next lemma, we suppose the following additional assumption

$$\Theta_D \in L^\infty(0, T_f; W^{\frac{2+s}{3+s}, 3+s}(\Gamma_D)), \qquad s > 0, \tag{35}$$

which is mainly needed because of the non-homogeneous Dirichlet boundary conditions on the temperature. Note that this assumption also implies that

$$\mathcal{R}_\Theta \in L^\infty(0, T_f; W^{2,3+s}(\Omega)).$$

Lemma 4. *Under the assumptions of Lemma 3 in a addition to $\lambda_1 < 2\lambda_0$ and for small enough Δt we have,*

$$\|e_\Theta^{N+1}\|^2 + \sum_{n=0}^{N}\left(\frac{1}{2}\|\overline{e}_\Theta^{n+1} - e_\Theta^n\|^2 + \|e_\Theta^{n+1} - \overline{e}_\Theta^{n+1}\|^2\right) + \Delta t\sum_{n=0}^{N}\left(\frac{\lambda_0}{2}|\overline{e}_\Theta^{n+1}|_1^2 + (2\lambda_0 - \lambda_1)|e_\Theta^{n+1}|_1^2 + \frac{\lambda_0}{2}|e_\Theta^{n+1} - \overline{e}_\Theta^{n+1}|_1^2\right) \leq C\Delta t. \quad (36)$$

Proof. Applying the Taylor expansion to the temperature derivative of (15) at t_{n+1} then subtracting (21) from it, setting $\varphi = 2\Delta t\overline{e}_\Theta^{n+1}$ and using the identity (24), we obtain

$$\begin{aligned}
\|\overline{e}_\Theta^{n+1}\|^2 - \|e_\Theta^n\|^2 + \|\overline{e}_\Theta^{n+1} - e_\Theta^n\|^2 + 2\Delta t\int_\Omega \lambda(\Theta_\mathcal{R}^n)\nabla\overline{e}_\Theta^{n+1}\cdot\nabla\overline{e}_\Theta^{n+1}\,d\boldsymbol{x} &= 2\Delta t\langle I_\Theta^n, \overline{e}_\Theta^{n+1}\rangle \\
&\quad - 2\Delta t\int_\Omega\left(\lambda(\Theta_\mathcal{R}(t_{n+1})) - \lambda(\Theta_\mathcal{R}^n)\right)\nabla\left(\Theta(t_{n+1}) + \mathcal{R}_\Theta(t_{n+1})\right)\cdot\nabla\overline{e}_\Theta^{n+1}\,d\boldsymbol{x} \\
&\quad - 2\Delta t\left(\int_\Omega(\boldsymbol{u}(t_{n+1})\cdot\nabla)\Theta(t_{n+1})\overline{e}_\Theta^{n+1}\,d\boldsymbol{x} - \int_\Omega(\overline{\boldsymbol{u}}^{n+1}\cdot\nabla)\overline{\Theta}^{n+1}\,\overline{e}_\Theta^{n+1}\,d\boldsymbol{x} - \int_\Omega\frac{1}{2}\overline{\Theta}^{n+1}\,\nabla\cdot\overline{\boldsymbol{u}}^{n+1}\,\overline{e}_\Theta^{n+1}\,d\boldsymbol{x}\right) \\
&\quad - 2\Delta t\left(\int_\Omega\boldsymbol{u}(t_{n+1})\cdot\nabla\mathcal{R}_\Theta(t_{n+1})\,\overline{e}_\Theta^{n+1}\,d\boldsymbol{x} - \int_\Omega\overline{\boldsymbol{u}}^{n+1}\cdot\nabla\mathcal{R}_\Theta^{n+1}\,\overline{e}_\Theta^{n+1}\,d\boldsymbol{x} - \int_\Omega\frac{1}{2}\mathcal{R}_\Theta^{n+1}\,\nabla\cdot\overline{\boldsymbol{u}}^{n+1}\,\overline{e}_\Theta^{n+1}\,d\boldsymbol{x}\right), \quad (37)
\end{aligned}$$

where I_Θ^n is the truncation error associated to Θ given by

$$I_\Theta^n = \frac{1}{\Delta t}\int_{t_n}^{t_{n+1}}(t - t_n)\partial_{tt}\Theta(t)dt.$$

Choosing $\varphi = 2\Delta t\, e_\Theta^{n+1}$ in (23), adding the result to (37) and considering the bounds of λ in (8), we obtain

$$\begin{aligned}
\|e_\Theta^{n+1}\|^2 - \|e_\Theta^n\|^2 + \|\overline{e}_\Theta^{n+1} - e_\Theta^n\|^2 + \|e_\Theta^{n+1} - \overline{e}_\Theta^{n+1}\|^2 + \Delta t\left(\lambda_0|\overline{e}_\Theta^{n+1}|_1^2 + (2\lambda_0 - \lambda_1)|e_\Theta^{n+1}|_1^2 + \lambda_0|e_\Theta^{n+1} - \overline{e}_\Theta^{n+1}|_1^2\right) \\
\leq \underbrace{-2\Delta t\left(\int_\Omega(\boldsymbol{u}(t_{n+1})\cdot\nabla)\Theta(t_{n+1})\overline{e}_\Theta^{n+1}\,d\boldsymbol{x} - \int_\Omega(\overline{\boldsymbol{u}}^{n+1}\cdot\nabla)\overline{\Theta}^{n+1}\,\overline{e}_\Theta^{n+1}\,d\boldsymbol{x} - \int_\Omega\frac{1}{2}\overline{\Theta}^{n+1}\,\nabla\cdot\overline{\boldsymbol{u}}^{n+1}\,\overline{e}_\Theta^{n+1}\,d\boldsymbol{x}\right)}_{=A_1} \\
\underbrace{-2\Delta t\left(\int_\Omega\boldsymbol{u}(t_{n+1})\cdot\nabla\mathcal{R}_\Theta(t_{n+1})\,\overline{e}_\Theta^{n+1}\,d\boldsymbol{x} - \int_\Omega\overline{\boldsymbol{u}}^{n+1}\cdot\nabla\mathcal{R}_\Theta^{n+1}\,\overline{e}_\Theta^{n+1}\,d\boldsymbol{x} - \int_\Omega\frac{1}{2}\mathcal{R}_\Theta^{n+1}\,\nabla\cdot\overline{\boldsymbol{u}}^{n+1}\,\overline{e}_\Theta^{n+1}\,d\boldsymbol{x}\right)}_{=A_2} \\
\underbrace{-2\Delta t\int_\Omega\left(\lambda(\Theta_\mathcal{R}(t_{n+1})) - \lambda(\Theta_\mathcal{R}^n)\right)\nabla\left(\Theta(t_{n+1}) + \mathcal{R}_\Theta(t_{n+1})\right)\cdot\nabla\overline{e}_\Theta^{n+1}\,d\boldsymbol{x}}_{=A_3} + \underbrace{2\Delta t\langle I_\Theta^n, \overline{e}_\Theta^{n+1}\rangle}_{=A_4} \\
\underbrace{+2\Delta t\int_\Omega\left(\lambda(\overline{\Theta}_\mathcal{R}^{n+1}) - \lambda(\Theta_\mathcal{R}^n)\right)\nabla\Theta(t_{n+1})\cdot\nabla e_\Theta^{n+1}\,d\boldsymbol{x}}_{=A_5}.
\end{aligned}$$

Next, the right-hand side terms are bounded separately. By noting that

$$\int_\Omega(\overline{\boldsymbol{u}}^{n+1}\cdot\nabla)\overline{\Theta}^{n+1}\,\overline{e}_\Theta^{n+1}\,d\boldsymbol{x} + \int_\Omega\overline{\Theta}^{n+1}\,\nabla\cdot\overline{\boldsymbol{u}}^{n+1}\,\overline{e}_\Theta^{n+1}\,d\boldsymbol{x} = -\int_\Omega(\overline{\boldsymbol{u}}^{n+1}\cdot\nabla)\overline{e}_\Theta^{n+1}\overline{\Theta}^{n+1}\,d\boldsymbol{x},$$

and using the properties (10) we have for the term A_1

$$\begin{aligned} A_1 &= -\Delta t\left(\int_\Omega (\boldsymbol{u}(t_{n+1})\cdot\nabla)\Theta(t_{n+1})\overline{e}_\Theta^{n+1}\,d\boldsymbol{x} - \int_\Omega (\overline{\boldsymbol{u}}^{n+1}\cdot\nabla)\overline{\Theta}^{n+1}\,\overline{e}_\Theta^{n+1}\,d\boldsymbol{x}\right)\\ &\quad +\Delta t\left(\int_\Omega (\boldsymbol{u}(t_{n+1})\cdot\nabla)\overline{e}_\Theta^{n+1}\Theta(t_{n+1})\,d\boldsymbol{x} - \int_\Omega (\overline{\boldsymbol{u}}^{n+1}\cdot\nabla)\overline{e}_\Theta^{n+1}\overline{\Theta}^{n+1}\,d\boldsymbol{x}\right), \qquad (38)\\ &= -\Delta t\int_\Omega (\overline{\boldsymbol{e}}_u^{n+1}\cdot\nabla)\Theta(t_{n+1})\overline{e}_\Theta^{n+1}\,d\boldsymbol{x} + \Delta t\int_\Omega (\overline{\boldsymbol{e}}_u^{n+1}\cdot\nabla)\overline{e}_\Theta^{n+1}\Theta(t_{n+1})\,d\boldsymbol{x},\\ &\overset{By\ (11)}{\leq} C\Delta t|\overline{\boldsymbol{e}}_u^{n+1}|_1\,|\Theta(t_{n+1})|_1\,|\overline{e}_\Theta^{n+1}|_1 + C\Delta t|\overline{\boldsymbol{e}}_u^{n+1}|_1\,|\Theta(t_{n+1})|_1\,|\overline{e}_\Theta^{n+1}|_1,\\ &\overset{By\ (25)}{\leq} C\Delta t|\overline{\boldsymbol{e}}_u^{n+1}|_1^2 + \frac{\lambda_0\Delta t}{10}|\overline{e}_\Theta^{n+1}|_1^2. \qquad (39)\end{aligned}$$

Similarly, the term A_2 is handled as

$$\begin{aligned} A_2 &= -\Delta t\int_\Omega (\overline{\boldsymbol{e}}_u^{n+1}\cdot\nabla)\mathcal{R}_\Theta(t_{n+1})\overline{e}_\Theta^{n+1}\,d\boldsymbol{x} + \Delta t\int_\Omega (\overline{\boldsymbol{e}}_u^{n+1}\cdot\nabla)\overline{e}_\Theta^{n+1}\mathcal{R}_\Theta(t_{n+1})\,d\boldsymbol{x},\\ &\overset{Using\ (11)}{\leq} C\Delta t|\overline{\boldsymbol{e}}_u^{n+1}|_1\,|\mathcal{R}_\Theta(t_{n+1})|_1\,|\overline{e}_\Theta^{n+1}|_1 + C\Delta t|\overline{\boldsymbol{e}}_u^{n+1}|_1\,|\mathcal{R}_\Theta(t_{n+1})|_1\,|\overline{e}_\Theta^{n+1}|_1,\\ &\overset{By\ (25)}{\leq} C\Delta t|\overline{\boldsymbol{e}}_u^{n+1}|_1^2 + \frac{\lambda_0\Delta t}{10}|\overline{e}_\Theta^{n+1}|_1^2. \qquad (40)\end{aligned}$$

It should be stressed that the terms A_1 and A_2 are the ones precluding the full first-order for the temperature estimates mainly due to the term $\Delta t|\overline{\boldsymbol{e}}_u^{n+1}|_1^2$. For the remaining terms A_3, A_4 and A_5, we have

$$\begin{aligned} A_3 &\overset{By\ (8)}{\leq} 2\lambda_2\Delta t\int_\Omega |\Theta(t_{n+1})-\Theta^n|\,|\nabla\Theta(t_{n+1})\cdot\nabla\overline{e}_\Theta^{n+1}|\,d\boldsymbol{x} + 2\lambda_2\Delta t\int_\Omega |\Theta(t_{n+1})-\Theta^n|\,|\nabla\mathcal{R}_\Theta(t_{n+1})\cdot\nabla\overline{e}_\Theta^{n+1}|\,d\boldsymbol{x},\\ &\overset{By\ (28)and(35)}{\leq} C\Delta t\|\Theta(t_{n+1})-\Theta^n\|\,|\overline{e}_\Theta^{n+1}|_1 \leq C(\Delta t)^2\int_{t_n}^{t_{n+1}}\|\partial_t\Theta\|^2dt + C\Delta t\|e_\Theta^n\|^2 + \frac{\lambda_0\Delta t}{10}|\overline{e}_\Theta^{n+1}|_1^2,\end{aligned}$$

$$\begin{aligned} A_4 &\leq C\Delta t\|I_\Theta^n\|_{-1}^2 + \frac{\lambda_0\Delta t}{K}|\overline{e}_\Theta^{n+1}|_1^2,\\ &\leq C(\Delta t)^2\int_{t_n}^{t_{n+1}}\|\partial_{tt}\Theta\|_{-1}^2dt + \frac{\lambda_0\Delta t}{10}|\overline{e}_\Theta^{n+1}|_1^2. \qquad (41)\end{aligned}$$

and

$$\begin{aligned} A_5 &\overset{By\ (8)\ and\ (28)}{\leq} C\lambda_2\Delta t\|\overline{\Theta}^{n+1}-\Theta^n\|\,|e_\Theta^{n+1}|_1 \leq C\lambda_2\Delta t\left(\|\overline{e}_\Theta^{n+1}-e_\Theta^n\| + \|\Theta(t_{n+1})-\Theta(t_n)\|\right)\left(|e_\Theta^{n+1}-\overline{e}_\Theta^{n+1}|_1 + |\overline{e}_\Theta^{n+1}|_1\right),\\ &\leq \frac{C\lambda_2^2}{\lambda_0}\Delta t\|\overline{e}_\Theta^{n+1}-e_\Theta^n\|^2 + C(\Delta t)^2\int_{t_n}^{t_{n+1}}\|\partial_t\Theta\|^2dt + \frac{\lambda_0\Delta t}{2}|e_\Theta^{n+1}-\overline{e}_\Theta^{n+1}|_1^2 + \frac{\lambda_0\Delta t}{10}|\overline{e}_\Theta^{n+1}|_1^2.\end{aligned}$$

Assembling the previous inequalities and summing over $n = 0, 1, \ldots, N$, we can write

$$\begin{aligned} &\|e_\Theta^{N+1}\|^2 + \sum_{n=0}^{N}\left(\|e_\Theta^{n+1}-\overline{e}_\Theta^{n+1}\|^2 + \|\overline{e}_\Theta^{n+1}-e_\Theta^n\|^2\right) + \Delta t\sum_{n=0}^{N}\left(\frac{\lambda_0}{2}|\overline{e}_\Theta^{n+1}|_1^2 + (2\lambda_0-\lambda_1)|e_\Theta^{n+1}|_1^2 + \frac{\lambda_0}{2}|e_\Theta^{n+1}-\overline{e}_\Theta^{n+1}|_1^2\right)\\ &\qquad \leq C\Delta t\sum_{n=0}^{N}|\overline{\boldsymbol{e}}_u^{n+1}|_1^2 + C\Delta t\sum_{n=0}^{N}\|e_\Theta^n\|^2 + C(\Delta t)^2\int_0^{T_f}\left(\|\partial_t\Theta\|^2 + \|\partial_{tt}\Theta\|_{-1}^2\right)dt + C\Delta t\sum_{n=0}^{N}\|\overline{e}_\Theta^{n+1}-e_\Theta^n\|^2. \qquad (42)\end{aligned}$$

Thanks to Lemma 3 we have

$$\Delta t\sum_{n=0}^{N}|\overline{\boldsymbol{e}}_u^{n+1}|_1^2 \leq C\Delta t + C\Delta t\sum_{n=0}^{N}\left(\|e_\Theta^n\|^2 + \|\overline{e}_\Theta^{n+1}-e_\Theta^n\|^2\right),$$

and for small enough Δt, it is possible to write

$$C\Delta t \sum_{n=0}^{N} \|\overline{e}_{\Theta}^{n+1} - e_{\Theta}^{n}\|^2 \leq \frac{1}{2} \sum_{n=0}^{N} \|\overline{e}_{\Theta}^{n+1} - e_{\Theta}^{n}\|^2.$$

Hence, the inequality (42) becomes

$$\|e_{\Theta}^{N+1}\|^2 + \sum_{n=0}^{N} \left(\|e_{\Theta}^{n+1} - \overline{e}_{\Theta}^{n+1}\|^2 + \frac{1}{2}\|\overline{e}_{\Theta}^{n+1} - e_{\Theta}^{n}\|^2 \right) + \Delta t \sum_{n=0}^{N} \left(\frac{\lambda_0}{2}|\overline{e}_{\Theta}^{n+1}|_1^2 + (2\lambda_0 - \lambda_1)|e_{\Theta}^{n+1}|_1^2 + \frac{\lambda_0}{2}|e_{\Theta}^{n+1} - \overline{e}_{\Theta}^{n+1}|_1^2 \right)$$
$$\leq C\Delta t + C\Delta t \sum_{n=0}^{N} \|e_{\Theta}^{n}\|^2,$$

where we have used (25). Finally, applying the Gronwall lemma 2 ends the poof. ∎

It should be noted that thanks to Lemma 3, we have for all $n = 0, 1, \ldots, N+1$

$$\|e_{\Theta}^{n}\|^2 \leq C\Delta t,$$

which means that

$$\Delta t \sum_{n=0}^{N} \|e_{\Theta}^{n}\|^2 \leq C\Delta t. \tag{43}$$

As we have seen in the above proof, the presence of the term $\Delta t \sum_{n=0}^{N} |\overline{e}_{u}^{n+1}|_1^2$ would degrade the order of the temperature error estimates allowing only a 1/2-order. Hence, this result along with (43) would enable to finalize the 1/2-order estimates of Lemma 3 which becomes:

Lemma 5. *Under the assumptions of Lemma 3 and Lemma 4, we have*

$$\|\boldsymbol{e}_{u}^{N+1}\|^2 + \sum_{n=0}^{N} \left(\|\overline{\boldsymbol{e}}_{u}^{n+1} - \boldsymbol{e}_{u}^{n}\|^2 + \frac{1}{2}\|\boldsymbol{e}_{u}^{n+1} - \overline{\boldsymbol{e}}_{u}^{n+1}\|^2 \right) + C_r\, \Delta t \sum_{n=0}^{N} \left(\nu_\infty |\overline{\boldsymbol{e}}_{u}^{n+1}|_1^2 + (2\nu_\infty - \nu_1)|\boldsymbol{e}_{u}^{n+1}|_1^2 + \nu_\infty |\boldsymbol{e}_{u}^{n+1} - \overline{\boldsymbol{e}}_{u}^{n+1}|_1^2 \right)$$
$$\leq C\Delta t. \tag{44}$$

The 1/2-order estimates being established for both velocity and temperature, we seek now to reach the full first-order estimates. This is achieved by the following theorem:

Theorem 1. *Under the assumpions of Lemma 3 and Lemma 4, we have*

$$\|\boldsymbol{e}_{u}^{N+1}\|^2 + \|e_{\Theta}^{N+1}\|^2 + \sum_{n=0}^{N} \left(\|\boldsymbol{e}_{u}^{n+1} - \boldsymbol{e}_{u}^{n}\|^2 + \|\overline{e}_{\Theta}^{n+1} - e_{\Theta}^{n}\|^2 + \|e_{\Theta}^{n+1} - \overline{e}_{\Theta}^{n+1}\|^2 \right) + C_r\, \nu_\infty\, \Delta t \sum_{n=0}^{N} |\boldsymbol{e}_{u}^{n+1}|_1^2$$
$$+ \Delta t \sum_{n=0}^{N} \left(\frac{\lambda_0}{2}|\overline{e}_{\Theta}^{n+1}|_1^2 + \frac{\lambda_0}{2}|e_{\Theta}^{n+1} - \overline{e}_{\Theta}^{n+1}|_1^2 + (2\lambda_0 - \lambda_1)|e_{\Theta}^{n+1}|_1^2 \right) \leq C(\Delta t)^2.$$

Proof. Adding (20) to (22), substructing the result from (31), we get

$$\int_\Omega \frac{\boldsymbol{e}_{u}^{n+1} - \boldsymbol{e}_{u}^{n}}{\Delta t} \cdot \boldsymbol{v}\, d\boldsymbol{x} + \int_\Omega 2\nu(\Theta_{\mathcal{R}}(t_{n+1}), \boldsymbol{Du}(t_{n+1}))\boldsymbol{Du}(t_{n+1}) : \boldsymbol{Dv}\, d\boldsymbol{x} - \int_\Omega 2\nu(\overline{\Theta}_{\mathcal{R}}^{n+1}, \boldsymbol{Du}^{n})\boldsymbol{Du}^{n+1} : \boldsymbol{Dv}\, d\boldsymbol{x}$$
$$= \alpha \int_\Omega \left(\boldsymbol{f}(\Theta_{\mathcal{R}}(t_{n+1})) - \boldsymbol{f}(\Theta_{\mathcal{R}}^{n}) \right) \cdot \boldsymbol{v}\, d\boldsymbol{x} + \int_\Omega p(t_{n+1}) \nabla \cdot \boldsymbol{v}\, d\boldsymbol{x} - \int_\Omega p^{n+1} \nabla \cdot \boldsymbol{v}\, d\boldsymbol{x} - \int_\Omega (\boldsymbol{u}(t_{n+1}) \cdot \nabla)\, \boldsymbol{u}(t_{n+1}) \cdot \boldsymbol{v}\, d\boldsymbol{x}$$
$$+ \int_\Omega (\boldsymbol{u}^{n} \cdot \nabla)\, \overline{\boldsymbol{u}}^{n+1} \cdot \boldsymbol{v}\, d\boldsymbol{x} + \langle \boldsymbol{I}_{u}^{n}, \boldsymbol{v} \rangle. \tag{45}$$

Setting $\boldsymbol{v} = 2\Delta t \boldsymbol{e}_u^{n+1}$, which is divgence-free, we obtain

$$
\begin{aligned}
&\|\boldsymbol{e}_u^{n+1}\|^2 - \|\boldsymbol{e}_u^{n}\|^2 + \|\boldsymbol{e}_u^{n+1} - \boldsymbol{e}_u^{n}\|^2 + 4\Delta t \int_\Omega \nu(\overline{\Theta}_{\mathcal{R}}^{n+1}, \boldsymbol{Du}^n)\boldsymbol{De}_u^{n+1} : \boldsymbol{De}_u^{n+1}\, d\boldsymbol{x} \\
&= 2\alpha\Delta t \int_\Omega (\boldsymbol{f}(\Theta_{\mathcal{R}}(t_{n+1})) - \boldsymbol{f}(\Theta_{\mathcal{R}}^n)) \cdot \boldsymbol{e}_u^{n+1}\, d\boldsymbol{x} - 4\Delta t \int_\Omega \Big(\nu(\Theta_{\mathcal{R}}(t_{n+1}), \boldsymbol{Du}(t_{n+1})) - \nu(\overline{\Theta}_{\mathcal{R}}^{n+1}, \boldsymbol{Du}^n)\Big)\boldsymbol{Du}(t_{n+1}) : \boldsymbol{De}_u^{n+1}\, d\boldsymbol{x} \\
&\qquad - 2\Delta t\left(\int_\Omega (\boldsymbol{u}(t_{n+1})\cdot\nabla)\boldsymbol{u}(t_{n+1})\cdot\boldsymbol{e}_u^{n+1}\, d\boldsymbol{x} - \int_\Omega (\boldsymbol{u}^n\cdot\nabla)\overline{\boldsymbol{u}}^{n+1}\cdot\boldsymbol{e}_u^{n+1}\, d\boldsymbol{x}\right) + 2\Delta t\langle \boldsymbol{I}_u^n, \boldsymbol{e}_u^{n+1}\rangle,
\end{aligned}
$$

where we have used (24). The assumptions (9) on ν and the Korn's inequality allow to write

$$
\begin{aligned}
\|\boldsymbol{e}_u^{n+1}\|^2 - \|\boldsymbol{e}_u^{n}\|^2 + \|\boldsymbol{e}_u^{n+1} - \boldsymbol{e}_u^{n}\|^2 + 4\,C_r\,\nu_\infty\,\Delta t|\boldsymbol{e}_u^{n+1}|_1^2 \le \underbrace{2\alpha\Delta t \int_\Omega (\boldsymbol{f}(\Theta_{\mathcal{R}}(t_{n+1})) - \boldsymbol{f}(\Theta_{\mathcal{R}}^n))\cdot\boldsymbol{e}_u^{n+1}\, d\boldsymbol{x}}_{=D_1} + \underbrace{2\Delta t\langle \boldsymbol{I}_u^n, \boldsymbol{e}_u^{n+1}\rangle}_{=D_2} \\
\underbrace{-4\Delta t \int_\Omega \Big(\nu(\Theta_{\mathcal{R}}(t_{n+1}), \boldsymbol{Du}(t_{n+1})) - \nu(\overline{\Theta}_{\mathcal{R}}^{n+1}, \boldsymbol{Du}^n)\Big)\boldsymbol{Du}(t_{n+1}) : \boldsymbol{De}_u^{n+1}\, d\boldsymbol{x}}_{=D_3} \\
\underbrace{-2\Delta t\left(\int_\Omega (\boldsymbol{u}(t_{n+1})\cdot\nabla)\boldsymbol{u}(t_{n+1})\cdot\boldsymbol{e}_u^{n+1}\, d\boldsymbol{x} - \int_\Omega (\boldsymbol{u}^n\cdot\nabla)\overline{\boldsymbol{u}}^{n+1}\cdot\boldsymbol{e}_u^{n+1}\, d\boldsymbol{x}\right)}_{=D_4}.
\end{aligned}
$$

Then, each term in the right-hand side is bounded separately as follows

$$
\begin{aligned}
D_1 &\le C\Delta t\left\|\int_{t_n}^{t_{n+1}} \partial_t\Theta(t)dt\right\|^2 + C\Delta t\|e_\Theta^n\|^2 + \frac{2\nu_\infty C_r\Delta t}{9}|\boldsymbol{e}_u^{n+1}|_1^2, \\
&\le C(\Delta t)^2\int_{t_n}^{t_{n+1}} \|\partial_t\Theta\|^2 dt + C\Delta t\|e_\Theta^n\|^2 + \frac{2\nu_\infty\Delta t}{9}|\boldsymbol{e}_u^{n+1}|_1^2,
\end{aligned}
$$

where the assumption (3) has been used along with the Poincaré inequality on $\boldsymbol{e}_u^{n+1}$. Next,

$$
\begin{aligned}
D_2 = 2\Delta t\langle \boldsymbol{I}_u^n, \boldsymbol{e}_u^{n+1}\rangle &\le \frac{C}{\Delta t}\left\|\int_{t_n}^{t_{n+1}} (t-t_n)\partial_{tt}\boldsymbol{u}(t)dt\right\|_{-1}^2 + \frac{2\nu_\infty C_r\Delta t}{9}|\boldsymbol{e}_u^{n+1}|_1^2, \\
&\le C(\Delta t)^2\int_{t_n}^{t_{n+1}} \|\partial_{tt}\boldsymbol{u}\|_{-1}^2 dt + \frac{2\nu_\infty C_r\Delta t}{9}|\boldsymbol{e}_u^{n+1}|_1^2.
\end{aligned}
$$

Following the approach detailed in Appendix A, the term D_3 is bounded by

$$
\begin{aligned}
D_3 &= -4\Delta t\int_\Omega \Big(\nu(\Theta_{\mathcal{R}}(t_{n+1}), \boldsymbol{Du}(t_{n+1})) - \nu(\overline{\Theta}_{\mathcal{R}}^{n+1}, \boldsymbol{Du}^n)\Big)\boldsymbol{Du}(t_{n+1}) : \boldsymbol{De}_u^{n+1}\, d\boldsymbol{x}, \\
&\le C\Delta t(\|\overline{e}_\Theta^{n+1} - e_\Theta^n\|^2 + \|e_\Theta^n\|^2) + C(\Delta t)^2\int_\Omega |\partial_t\boldsymbol{u}|_1^2 dt + \frac{36\,C_u^2\,C_\nu^2}{\nu_\infty C_r}\Delta t|\boldsymbol{e}_u^n|_1^2 + 4\frac{\nu_\infty C_r\Delta t}{9}|\boldsymbol{e}_u^{n+1}|_1^2.
\end{aligned}
$$

The term D_4 is first split, using the properties (10), into four terms $D_{4,1}, D_{4,2}, D_{4,3}$ and $D_{4,4}$ as

$$
\begin{aligned}
D_4 &= -2\Delta t\int_\Omega (\boldsymbol{u}(t_{n+1})\cdot\nabla)\,\boldsymbol{u}(t_{n+1})\cdot\boldsymbol{e}_u^{n+1}\, d\boldsymbol{x} + \int_\Omega (\boldsymbol{u}^n\cdot\nabla)\,\overline{\boldsymbol{u}}^{n+1}\cdot\boldsymbol{e}_u^{n+1}\, d\boldsymbol{x}, \\
&= \underbrace{-2\Delta t\int_\Omega ((\boldsymbol{u}(t_{n+1}) - \boldsymbol{u}(t_n))\cdot\nabla)\,\boldsymbol{u}(t_{n+1})\cdot\boldsymbol{e}_u^{n+1}\, d\boldsymbol{x}}_{=D_{4,1}} \underbrace{-2\Delta t\int_\Omega (\boldsymbol{e}_u^n\cdot\nabla)\boldsymbol{u}(t_{n+1})\cdot\boldsymbol{e}_u^{n+1}\, d\boldsymbol{x}}_{=D_{4,2}}, \\
&\underbrace{+2\Delta t\int_\Omega (\boldsymbol{u}(t_n)\cdot\nabla)\boldsymbol{e}_u^{n+1}\cdot\overline{\boldsymbol{e}}_u^{n+1}\, d\boldsymbol{x}}_{=D_{4,3}} \underbrace{-2\Delta t\int_\Omega (\boldsymbol{e}_u^n\cdot\nabla)\boldsymbol{e}_u^{n+1}\cdot\overline{\boldsymbol{e}}_u^{n+1}\, d\boldsymbol{x}}_{=D_{4,4}},
\end{aligned}
$$

then each term is separately bounded as follows

$$\begin{aligned} D_{4,1} &= -2\Delta t \int_\Omega ((\boldsymbol{u}(t_{n+1}) - \boldsymbol{u}(t_n)) \cdot \nabla)\, \boldsymbol{u}(t_{n+1}) \cdot \boldsymbol{e}_u^{n+1}\, d\boldsymbol{x}, \\ &\overset{\text{By (11)}}{\leq} C\Delta t \|\boldsymbol{u}(t_{n+1}) - \boldsymbol{u}(t_n)\|\, \|\boldsymbol{u}(t_{n+1})\|_2\, |\boldsymbol{e}_u^{n+1}|_1, \\ &\overset{\text{By (26)}}{\leq} C\Delta t \|\boldsymbol{u}(t_{n+1}) - \boldsymbol{u}(t_n)\|\, |\boldsymbol{e}_u^{n+1}|_1, \\ &\leq C(\Delta t)^2 \int_{t_n}^{t_{n+1}} \|\partial_t \boldsymbol{u}\|^2 dt + \frac{2\nu_\infty C_r \Delta t}{9} |\boldsymbol{e}_u^{n+1}|_1^2, \end{aligned}$$

$$\begin{aligned} D_{4,2} &= -2\Delta t \int_\Omega (\boldsymbol{e}_u^n \cdot \nabla)\boldsymbol{u}(t_{n+1}) \cdot \boldsymbol{e}_u^{n+1}\, d\boldsymbol{x}, \\ &\leq C\Delta t \|\boldsymbol{e}_u^n\|\, \|\boldsymbol{u}(t_{n+1})\|_2\, |\boldsymbol{e}_u^{n+1}|_1, \\ &\overset{\text{By (26)}}{\leq} C\Delta t \|\boldsymbol{e}_u^n\|\, |\boldsymbol{e}_u^{n+1}|_1, \\ &\leq C\Delta t \|\boldsymbol{e}_u^n\|^2 + \frac{2\nu_\infty C_r \Delta t}{9} |\boldsymbol{e}_u^{n+1}|_1^2, \end{aligned}$$

$$\begin{aligned} D_{4,3} &= 2\Delta t \int_\Omega (\boldsymbol{u}(t_n) \cdot \nabla)\boldsymbol{e}_u^{n+1} \cdot \overline{\boldsymbol{e}}_u^{n+1}\, d\boldsymbol{x}, \\ &\leq C\Delta t \|\boldsymbol{u}(t_n)\|_2\, |\boldsymbol{e}_u^{n+1}|_1\, \|\overline{\boldsymbol{e}}_u^{n+1}\|, \\ &\leq C\Delta t |\boldsymbol{e}_u^{n+1}|_1\, \|\overline{\boldsymbol{e}}_u^{n+1}\|, \\ &\leq C\Delta t (\|\overline{\boldsymbol{e}}_u^{n+1} - \boldsymbol{e}_u^n\|^2 + \|\boldsymbol{e}_u^n\|^2) + \frac{2\nu_\infty C_r \Delta t}{9} |\boldsymbol{e}_u^{n+1}|_1^2, \end{aligned}$$

$$\begin{aligned} D_{4,4} &= -2\Delta t \int_\Omega (\boldsymbol{e}_u^n \cdot \nabla)\boldsymbol{e}_u^{n+1} \cdot \overline{\boldsymbol{e}}_u^{n+1}\, d\boldsymbol{x}, \\ &\overset{\text{By (11)}}{\leq} C\Delta t |\boldsymbol{e}_u^n|_1^{\frac{1}{2}}\, \|\boldsymbol{e}_u^n\|^{\frac{1}{2}} |\boldsymbol{e}_u^{n+1}|_1\, |\overline{\boldsymbol{e}}_u^{n+1}|_1, \\ &\leq C\Delta t |\boldsymbol{e}_u^n|_1\, \|\boldsymbol{e}_u^n\|\, |\overline{\boldsymbol{e}}_u^{n+1}|_1^2 + \frac{2\nu_\infty C_r \Delta t}{9} |\boldsymbol{e}_u^{n+1}|_1^2 \leq C\Delta t \|\boldsymbol{e}_u^n\|^2 + \frac{\nu_\infty C_r \Delta t}{2} |\boldsymbol{e}_u^n|_1^2 + \frac{2\nu_\infty C_r \Delta t}{9} |\boldsymbol{e}_u^{n+1}|_1^2, \end{aligned}$$

where we have used $|\overline{\boldsymbol{e}}_u^{n+1}|_1 \leq C$ that results from Lemma 5. Assembling the previous inequalities and summing over $n = 0, 1, \ldots, N$, we obtain

$$\begin{aligned} \|\boldsymbol{e}_u^{N+1}\|^2 + \sum_{n=0}^{N} \|\boldsymbol{e}_u^{n+1} - \boldsymbol{e}_u^n\|^2 + 2\, C_r\, \nu_\infty\, \Delta t \sum_{n=0}^{N} |\boldsymbol{e}_u^{n+1}|_1^2 &\leq C\Delta t \sum_{n=0}^{N} \|\boldsymbol{e}_u^n\|^2 + C\Delta t \sum_{n=0}^{N} \|\overline{\boldsymbol{e}}_u^{n+1} - \boldsymbol{e}_u^n\|^2 + \frac{\nu_\infty C_r \Delta t}{2} \sum_{n=0}^{N} |\boldsymbol{e}_u^n|_1^2 \\ + C(\Delta t)^2 \int_0^{T_f} \left(\|\partial_t \boldsymbol{u}\|^2 + |\partial_t \boldsymbol{u}|_1^2 + \|\partial_{tt} \boldsymbol{u}\|_{-1}^2 + \|\partial_t \Theta\|^2 \right) dt + C\Delta t \sum_{n=0}^{N} (\|\overline{e}_\Theta^{n+1} - e_\Theta^n\|^2 + \|e_\Theta^n\|^2) \\ + \frac{36\, C_u^2\, C_\nu^2}{\nu_\infty C_r} \Delta t \sum_{n=0}^{N} |\boldsymbol{e}_u^n|_1^2. \end{aligned}$$

The assumptions (26), (25) along with the estimates of Lemma 5 and Lemma 4 allow to write

$$\|\boldsymbol{e}_u^{N+1}\|^2 + \sum_{n=0}^{N} \|\boldsymbol{e}_u^{n+1} - \boldsymbol{e}_u^n\|^2 + C_r\, \nu_\infty\, \Delta t |\boldsymbol{e}_u^{N+1}|_1^2 + C_r\, \nu_\infty\, \Delta t \sum_{n=0}^{N} |\boldsymbol{e}_u^{n+1}|_1^2 \leq C(\Delta t)^2 + C\Delta t \sum_{n=0}^{N} \|\boldsymbol{e}_u^n\|^2 + C\Delta t \sum_{n=0}^{N} \|e_\Theta^n\|^2, \quad (46)$$

where we have also used the assumption (29) to have $\frac{36\,C_u^2\,C_\nu^2}{\nu_\infty C_r} \leq \frac{\nu_\infty C_r}{2}$. On the other hand, as mentioned before, $\Delta t|\bar{\boldsymbol{e}}_u^{n+1}|_1^2$ is the only term degrading the order of temperature error estimates in Lemma 4. The idea here is to make the term $\Delta t\|\bar{\boldsymbol{e}}_u^{n+1}\|^2$ appears instead of the abovementioned problematic term. Note that, according to the proof of Lemma 4, the problematic term is originated from the bounds of the terms A_1 in (38) and A_2 in (40). Therefore, we will reproduce the same steps as in the proof of Lemma4 except for the terms of interest A_1 and A_2 which are now bounded as follows

$$\begin{aligned} A_1 &= -\Delta t\int_\Omega(\bar{\boldsymbol{e}}_u^{n+1}\cdot\nabla)\Theta(t_{n+1})\bar{e}_\Theta^{n+1}\,d\boldsymbol{x}+\Delta t\int_\Omega(\bar{\boldsymbol{e}}_u^{n+1}\cdot\nabla)\bar{e}_\Theta^{n+1}\Theta(t_{n+1})\,d\boldsymbol{x},\\ &\overset{\text{By (11)}}{\leq} C\Delta t\|\bar{\boldsymbol{e}}_u^{n+1}\|\,\|\Theta(t_{n+1})\|_2\,|\bar{e}_\Theta^{n+1}|_1+C\Delta t\|\bar{\boldsymbol{e}}_u^{n+1}\|\,|\bar{e}_\Theta^{n+1}|_1\,\|\Theta(t_{n+1})\|_2,\\ &\overset{\text{By (25)}}{\leq} C\Delta t\|\bar{\boldsymbol{e}}_u^{n+1}\|^2+\frac{\lambda_0\Delta t}{12}|\bar{e}_\Theta^{n+1}|_1^2, \end{aligned}$$

and

$$\begin{aligned} A_2 &= -\Delta t\int_\Omega(\bar{\boldsymbol{e}}_u^{n+1}\cdot\nabla)\mathcal{R}_\Theta(t_{n+1})\bar{e}_\Theta^{n+1}\,d\boldsymbol{x}+\Delta t\int_\Omega(\bar{\boldsymbol{e}}_u^{n+1}\cdot\nabla)\bar{e}_\Theta^{n+1}\mathcal{R}_\Theta(t_{n+1})\,d\boldsymbol{x},\\ &\overset{\text{By (11)}}{\leq} C\Delta t\|\bar{\boldsymbol{e}}_u^{n+1}\|\,\|\mathcal{R}_\Theta(t_{n+1})\|_2|\bar{e}_\Theta^{n+1}|_1+C\Delta t\|\bar{\boldsymbol{e}}_u^{n+1}\|\,|\bar{e}_\Theta^{n+1}|_1\,\|\mathcal{R}_\Theta(t_{n+1})\|_2,\\ &\overset{\text{By (35)}}{\leq} C\Delta t\|\bar{\boldsymbol{e}}_u^{n+1}\|^2+\frac{\lambda_0\Delta t}{12}|\bar{e}_\Theta^{n+1}|_1^2, \end{aligned}$$

which yields the following inequality

$$\begin{aligned} &\|e_\Theta^{N+1}\|^2+\sum_{n=0}^N\Big(\|\bar{e}_\Theta^{n+1}-e_\Theta^n\|^2+\|e_\Theta^{n+1}-\bar{e}_\Theta^{n+1}\|^2\Big)+\Delta t\sum_{n=0}^N\Big(\frac{\lambda_0}{2}|\bar{e}_\Theta^{n+1}|_1^2+\frac{\lambda_0}{2}|e_\Theta^{n+1}-\bar{e}_\Theta^{n+1}|_1^2+(2\lambda_0-\lambda_1)|e_\Theta^{n+1}|_1^2\Big)\\ &\qquad\leq C\Delta t\sum_{n=0}^N\|\bar{\boldsymbol{e}}_u^{n+1}\|^2+C\Delta t\sum_{n=0}^N\|e_\Theta^n\|^2+C\Delta t\sum_{n=0}^N\|\bar{e}_\Theta^{n+1}-e_\Theta^n\|^2+C(\Delta t)^2\int_0^{T_f}\Big(\|\partial_t\Theta\|^2+\|\partial_{tt}\Theta\|_{-1}^2\Big)dt. \quad (47) \end{aligned}$$

Thus, we have from Lemma 5

$$C\Delta t\sum_{n=0}^N\|\bar{\boldsymbol{e}}_u^{n+1}\|^2\leq C\Delta t\sum_{n=0}^N\|\boldsymbol{e}_u^{n+1}-\bar{\boldsymbol{e}}_u^{n+1}\|^2+C\Delta t\sum_{n=0}^N\|\boldsymbol{e}_u^{n+1}\|^2\leq C(\Delta t)^2+C\Delta t\sum_{n=0}^N\|\boldsymbol{e}_u^{n+1}\|^2,$$

and using Lemma 4 in addition to the assumptions (25), the inequality (47) becomes

$$\begin{aligned} &\|e_\Theta^{N+1}\|^2+\sum_{n=0}^N\Big(\|\bar{e}_\Theta^{n+1}-e_\Theta^n\|^2+\|e_\Theta^{n+1}-\bar{e}_\Theta^{n+1}\|^2\Big)+\Delta t\sum_{n=0}^N\Big(\frac{\lambda_0}{2}|\bar{e}_\Theta^{n+1}|_1^2+\frac{\lambda_0}{2}|e_\Theta^{n+1}-\bar{e}_\Theta^{n+1}|_1^2+(2\lambda_0-\lambda_1)|e_\Theta^{n+1}|_1^2\Big)\\ &\qquad\leq C(\Delta t)^2+C\Delta t\sum_{n=0}^N\|\boldsymbol{e}_u^{n+1}\|^2+C\Delta t\sum_{n=0}^N\|e_\Theta^n\|^2. \quad (48) \end{aligned}$$

Adding (47) to (46) we obtain

$$\begin{aligned} &\|\boldsymbol{e}_u^{N+1}\|^2+\|e_\Theta^{N+1}\|^2+\sum_{n=0}^N\Big(\|\boldsymbol{e}_u^{n+1}-\boldsymbol{e}_u^n\|^2+\|\bar{e}_\Theta^{n+1}-e_\Theta^n\|^2+\|e_\Theta^{n+1}-\bar{e}_\Theta^{n+1}\|^2\Big)+C_r\,\nu_\infty\,\Delta t|\boldsymbol{e}_u^{N+1}|_1^2+\,2C_r\,\nu_\infty\,\Delta t\sum_{n=0}^N|\boldsymbol{e}_u^{n+1}|_1^2\\ &+\Delta t\sum_{n=0}^N\Big(\frac{\lambda_0}{2}|\bar{e}_\Theta^{n+1}|_1^2+\frac{\lambda_0}{2}|e_\Theta^{n+1}-\bar{e}_\Theta^{n+1}|_1^2+(2\lambda_0-\lambda_1)|e_\Theta^{n+1}|_1^2\Big)\leq C(\Delta t)^2+C\Delta t\sum_{n=0}^N\|\boldsymbol{e}_u^n\|^2+C\Delta t\sum_{n=0}^N\|\boldsymbol{e}_u^{n+1}\|^2+C\Delta t\sum_{n=0}^N\|e_\Theta^n\|^2. \end{aligned}$$

Applying the discrete Gronwall lemma 2, we get

$$\|\boldsymbol{e}_u^{N+1}\|^2 + \|e_\Theta^{N+1}\|^2 + \sum_{n=0}^{N}\left(\|\boldsymbol{e}_u^{n+1}-\boldsymbol{e}_u^{n}\|^2 + \|\bar{e}_\Theta^{n+1}-e_\Theta^{n}\|^2 + \|e_\Theta^{n+1}-\bar{e}_\Theta^{n+1}\|^2\right) + 2C_r\,\nu_\infty\,\Delta t\sum_{n=0}^{N}|\boldsymbol{e}_u^{n+1}|_1^2$$
$$+\,\Delta t\sum_{n=0}^{N}\left(\frac{\lambda_0}{2}|\bar{e}_\Theta^{n+1}|_1^2 + \frac{\lambda_0}{2}|e_\Theta^{n+1}-\bar{e}_\Theta^{n+1}|_1^2 + (2\lambda_0-\lambda_1)|e_\Theta^{n+1}|_1^2\right) \le C(\Delta t)^2. \quad \blacksquare$$

The next Theorem provides the $1/2$-order error estimate for the pressure approximation in the $L^2\left(0,T_f;L^2(\Omega)\right)$-norm.

Theorem 2. *Under the assumptions of Lemma 3 and Lemma 4, we have*

$$\left(\sum_{n=0}^{N}\Delta t\left\|p(t_{n+1})-p^{n+1}\right\|^2\right)^{1/2} \le C\,(\Delta t)^{1/2}. \tag{49}$$

Proof. From (45), we have

$$\int_\Omega\left(p(t_{n+1})-p^{n+1}\right)\nabla\cdot\boldsymbol{v}\;d\boldsymbol{x} = \int_\Omega\frac{\boldsymbol{e}_u^{n+1}-\boldsymbol{e}_u^{n}}{\Delta t}\cdot\boldsymbol{v}\;d\boldsymbol{x} - \alpha\int_\Omega\left(\boldsymbol{f}(\Theta_{\mathcal{R}}(t_{n+1}))-\boldsymbol{f}(\Theta_{\mathcal{R}}^n)\right)\cdot\boldsymbol{v}\;d\boldsymbol{x} + \int_\Omega 2\nu(\overline{\Theta}_{\mathcal{R}}^{n+1},\boldsymbol{D}\boldsymbol{u}^n)\boldsymbol{D}\boldsymbol{e}^{n+1}:\boldsymbol{D}\boldsymbol{v}\;d\boldsymbol{x}$$
$$-\langle\boldsymbol{I}_u^n,\boldsymbol{v}\rangle + \left(\int_\Omega(\boldsymbol{u}(t_{n+1})\cdot\nabla)\,\boldsymbol{u}(t_{n+1})\cdot\boldsymbol{v}\;d\boldsymbol{x} - \int_\Omega(\boldsymbol{u}^n\cdot\nabla)\,\overline{\boldsymbol{u}}^{n+1}\cdot\boldsymbol{v}\;d\boldsymbol{x}\right)$$
$$+\int_\Omega\left(2\nu(\Theta_{\mathcal{R}}(t_{n+1}),\boldsymbol{D}\boldsymbol{u}(t_{n+1}))-2\nu(\overline{\Theta}_{\mathcal{R}}^{n+1},\boldsymbol{D}\boldsymbol{u}^n)\right)\boldsymbol{D}\boldsymbol{u}(t_{n+1}):\boldsymbol{D}\boldsymbol{v}\;d\boldsymbol{x}. \tag{50}$$

The Inf-Sup condition (see for instance [22]) ensures

$$\left\|p(t_{n+1})-p^{n+1}\right\| \le C\sup_{\boldsymbol{v}\in\boldsymbol{H}_0^1(\Omega}\frac{\int_\Omega\left(p(t_{n+1})-p^{n+1}\right)\nabla\cdot\boldsymbol{v}\;d\boldsymbol{x}}{|v|_1}.$$

On the other, we can upper-bound the right-hand side terms of (50) as follows

$$\int_\Omega\frac{\boldsymbol{e}_u^{n+1}-\boldsymbol{e}_u^{n}}{\Delta t}\cdot\boldsymbol{v}\;d\boldsymbol{x} \le C\left\|\frac{\boldsymbol{e}_u^{n+1}-\boldsymbol{e}_u^{n}}{\Delta t}\right\||\boldsymbol{v}|_1, \qquad \text{(By Cauchy-Schwarz and Poincaré inequalities).}$$

$$-\alpha\int_\Omega\left(\boldsymbol{f}(\Theta_{\mathcal{R}}(t_{n+1}))-\boldsymbol{f}(\Theta_{\mathcal{R}}^n)\right)\cdot\boldsymbol{v}\;d\boldsymbol{x} \overset{\text{By (3)}}{\le} \left(\Delta t\int_{t_n}^{t_{n+1}}\|\partial_t\Theta\|^2dt\right)^{\frac{1}{2}}|\boldsymbol{v}|_1 + \|e_\Theta^n\|\,|\boldsymbol{v}|_1,$$
$$\int_\Omega 2\nu(\overline{\Theta}_{\mathcal{R}}^{n+1},\boldsymbol{D}\boldsymbol{u}^n)\boldsymbol{D}\boldsymbol{e}^{n+1}:\boldsymbol{D}\boldsymbol{v}\;d\boldsymbol{x} \overset{\text{By (9)}}{\le} \nu_1|\boldsymbol{e}^{n+1}|_1\,|\boldsymbol{v}|_1,$$
$$\langle\boldsymbol{I}_u^n,\boldsymbol{v}\rangle \le \|\boldsymbol{I}_u^n\|_{-1}|\boldsymbol{v}|_1 \le \left(\Delta t\int_{t_n}^{t_{n+1}}\|\partial_{tt}\boldsymbol{u}\|_{-1}^2dt\right)^{\frac{1}{2}}|\boldsymbol{v}|_1.$$

As for the nonlinear term, it is first split into three terms as follows

$$\int_\Omega(\boldsymbol{u}(t_{n+1})\cdot\nabla)\,\boldsymbol{u}(t_{n+1})\cdot\boldsymbol{v}\;d\boldsymbol{x} - \int_\Omega(\boldsymbol{u}^n\cdot\nabla)\,\overline{\boldsymbol{u}}^{n+1}\cdot\boldsymbol{v}\;d\boldsymbol{x} = \int_\Omega(\boldsymbol{u}(t_{n+1})-\boldsymbol{u}(t_n)\cdot\nabla)\,\boldsymbol{u}(t_{n+1})\cdot\boldsymbol{v}\;d\boldsymbol{x} +$$
$$\int_\Omega(\boldsymbol{e}_u^n\cdot\nabla)\boldsymbol{u}(t_{n+1})\cdot\boldsymbol{v}\;d\boldsymbol{x} + \int_\Omega(\boldsymbol{u}^n\cdot\nabla)\,\bar{\boldsymbol{e}}_u^{n+1}\cdot\boldsymbol{v}\;d\boldsymbol{x},$$

then bounded, using the inequalities (11), as

$$\int_\Omega (\boldsymbol{u}(t_{n+1}) - \boldsymbol{u}(t_n) \cdot \nabla)\, \boldsymbol{u}(t_{n+1}) \cdot \boldsymbol{v}\; d\boldsymbol{x} \le C\|\boldsymbol{u}(t_{n+1}) - \boldsymbol{u}(t_n)\|\, \|\boldsymbol{u}(t_{n+1})\|_2 |\boldsymbol{v}|_1 \overset{\text{By (26)}}{\le} C\left(\Delta t \int_{t_n}^{t_{n+1}} \|\partial_t \boldsymbol{u}\|^2 dt\right)^{\frac{1}{2}} |\boldsymbol{v}|_1,$$

$$\int_\Omega (\boldsymbol{e}_u^n \cdot \nabla)\boldsymbol{u}(t_{n+1}) \cdot \boldsymbol{v}\; d\boldsymbol{x} \le C|\boldsymbol{e}_u^n|_1 |\boldsymbol{u}(t_{n+1})|_1 |\boldsymbol{v}|_1 \overset{\text{Using (26)}}{\le} C|\boldsymbol{e}_u^n|_1 |\boldsymbol{v}|_1,$$

$$\begin{aligned}
\int_\Omega (\boldsymbol{u}^n \cdot \nabla)\, \overline{\boldsymbol{e}}_u^{n+1} \cdot \boldsymbol{v} \quad &\overset{\text{By (10)}}{=} \quad -\int_\Omega (\boldsymbol{e}_u^n \cdot \nabla)\overline{\boldsymbol{e}}_u^{n+1} \cdot \boldsymbol{v} - \int_\Omega (\boldsymbol{u}(t_n) \cdot \nabla)\boldsymbol{v} \cdot \overline{\boldsymbol{e}}_u^{n+1} \\
&\le \quad C|\boldsymbol{e}_u^n|_1\, |\overline{\boldsymbol{e}}_u^{n+1}|_1\, |\boldsymbol{v}|_1 + C\|\boldsymbol{u}(t_n)\|_2\, |\boldsymbol{v}|_1\, \|\overline{\boldsymbol{e}}_u^{n+1}\| \\
&\le \quad C|\boldsymbol{e}_u^n|_1\, |\boldsymbol{v}|_1 + C|\boldsymbol{v}|_1\, \|\overline{\boldsymbol{e}}_u^{n+1}\|,
\end{aligned}$$

where we have used $|\overline{\boldsymbol{e}}_u^{n+1}|_1 \le C$ given by Lemma 5. Following the argument detailed in Appendix A, we achieve

$$\int_\Omega \left(2\nu(\Theta_{\mathcal{R}}(t_{n+1}), \boldsymbol{Du}(t_{n+1})) - 2\nu(\overline{\Theta}_{\mathcal{R}}^{n+1}, \boldsymbol{Du}^n)\right) \boldsymbol{Du}(t_{n+1}) : \boldsymbol{Dv}\; d\boldsymbol{x} \quad \le \quad C\left(\|\overline{e}_\Theta^{n+1}\| + \left(\Delta t \int_{t_n}^{t_{n+1}} |\partial_t \boldsymbol{u}|_1^2\; dt\right)^{\frac{1}{2}} + |\boldsymbol{e}_u^n|_1\right) |\boldsymbol{v}|_1.$$

Assembling the above inequalities, we get

$$\begin{aligned}
\Delta t\|p(t_{n+1}) - p^{n+1}\|^2 \le \frac{1}{\Delta t}\|\boldsymbol{e}_u^{n+1} - \boldsymbol{e}_u^n\|^2 + C\Delta t\left(|\boldsymbol{e}_u^{n+1}|_1^2 + \|\overline{\boldsymbol{e}}_u^{n+1}\|^2 + |\boldsymbol{e}_u^n|_1^2 + \|\overline{e}_\Theta^{n+1}\|^2 + \|e_\Theta^n\|^2\right) \\
+ C(\Delta t)^2 \int_{t_n}^{t_{n+1}} (\|\partial_{tt}\boldsymbol{u}\|_{-1}^2 + \|\partial_t \boldsymbol{u}\|^2) dt + C(\Delta t)^2 \int_{t_n}^{t_{n+1}} \|\partial_t \Theta\|^2 dt.
\end{aligned}$$

Finally, taking the sum over $n = 0, 1, \ldots, N$ and using the estimates of Lemma 5 and Lemma 4 and Theorem 1 along with the assumptions (26) and (25), end the proof. ■

5. Numerical results and examples

Two examples are presented in this section to assess the computational performance of the proposed fractional time-stepping method for solving unsteady thermal convection in non-Newtonian fluids. In the first example, we solve the three-dimensional equations (4) with manufactured exact solutions to validate the theoretical error estimates established in this study for the semi-discrete velocity, temperature, and pressure solutions. In the second example, we apply the proposed method for solving the two-dimensional benchmark problem of thermal flow past a circular cylinder with nonlinear fluid viscosity and thermal conductivity coefficients depending on the velocity and temperature solutions. The third example solves a flow problem of natural convection of power-law fluids in a square enclosure with differentially heated side walls. In all considered examples, the well-established Taylor-Hood $\mathbb{P}_2/\mathbb{P}_1$ mixed finite elements are implemented for the spatial discretization for which the quadratic $\mathbb{P}_2$ finite elements are used for the velocity $\boldsymbol{u}$ and temperature Θ whereas the linear $\mathbb{P}_1$ finite elements are used for the pressure p. It should also be noted that this class of mixed finite elements satisfies the inf-sup condition required in Step 3 of the fractional time-stepping method. In our computations reported in this section, the resulting linear systems of algebraic equations are solved using the Generalized Minimal Residual (GMRES) iterative solver with a tolerance of 10^{-7} to stop the iterations.

5.1. Accuracy example

To examine the accuracy of the proposed fractional time-stepping method and its theoretical error estimates, we consider a test example with known analytical solutions. Thus, we solve the three-dimensional equations (4) in the

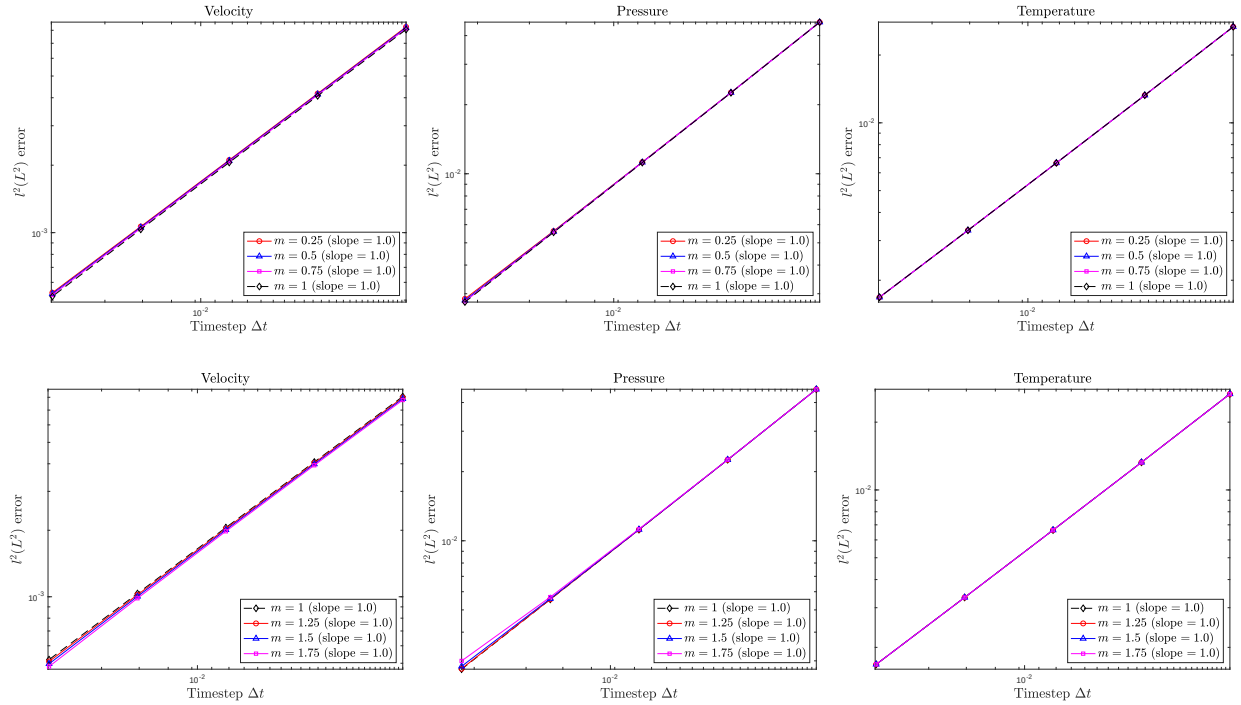

Figure 1: Convergence results using the $l^2(L^2)$-error for the velocity $\boldsymbol{u}$ (first column), pressure p (second column) and temperature Θ (third column) obtained for the accuracy example using $m \leq 1$ (first row) and $m \geq 1$ (second row).

spatial domain $\Omega = [0,1]^3$ subject to Dirichlet-type boundary conditions and temperature-dependent viscosity and thermal conductivity defined by

$$\nu(\Theta, \boldsymbol{Du}) = \nu_\infty + (\gamma(\Theta) - \nu_\infty)\left(1 + \beta_0^2 \|\boldsymbol{Du}\|^2_{\mathbb{R}^{3\times3}}\right)^{\frac{m-1}{2}},$$

with

$$\gamma(\Theta) = 10^{-4}\left(1 + \sin^2(\Theta)\right), \qquad \lambda(\Theta) = 10^{-4} e \frac{\ln(1+\Theta)}{1+\Theta}, \tag{51}$$

where $\beta_0 = 1$, $\nu_\infty = 5 \times 10^{-5}$, $\alpha = 10$ and the power index $m = 0.25, 0.5, 0.75, 1, 1.25, 1.5$ and 1.75. The boundary and initial functions are defined such that the analytical solution of the system (4) is given by

$$\begin{aligned}
u_1(t,x,y,z) &= \left(2x + 3xy - 2xz + x^2 - 0.5z^2\right)(1 - \cos(2t))\, e^{-t}, \\
u_2(t,x,y,z) &= -\left(-2y - xy + yz - 2y^2 - x^2\right)(1 - \cos(2t))\, e^{-t}, \\
u_3(t,x,y,z) &= \left(yz - xz + 0.5z^2 + 2y^2\right)(1 - \cos(2t))\, e^{-2t}, \\
p(t,x,y,z) &= (x - 2y + z)(1 - \cos(2t))\, e^{-t}, \\
\Theta(t,x,y,z) &= 1 + \left(2x^2 + y^2 + 3z^2 + 0.5\right)(1 - \cos(2t))\, e^{-t}.
\end{aligned} \tag{52}$$

Hence, using these exact solutions and (51), expressions of the source terms $\boldsymbol{f}$ and g in (4) are calculated as

$$\begin{aligned}
\boldsymbol{f} &= \frac{\partial \boldsymbol{u}}{\partial t} + (\boldsymbol{u}\cdot\nabla)\,\boldsymbol{u} - \nabla\cdot(2\nu(\Theta, \boldsymbol{Du})\boldsymbol{Du}) + \nabla p - 10\left(1 - e^{-\Theta}\right), \\
g &= \frac{\partial \Theta}{\partial t} + (\boldsymbol{u}\cdot\nabla)\,\Theta - \nabla\cdot(\lambda(\Theta)\nabla\Theta).
\end{aligned}$$

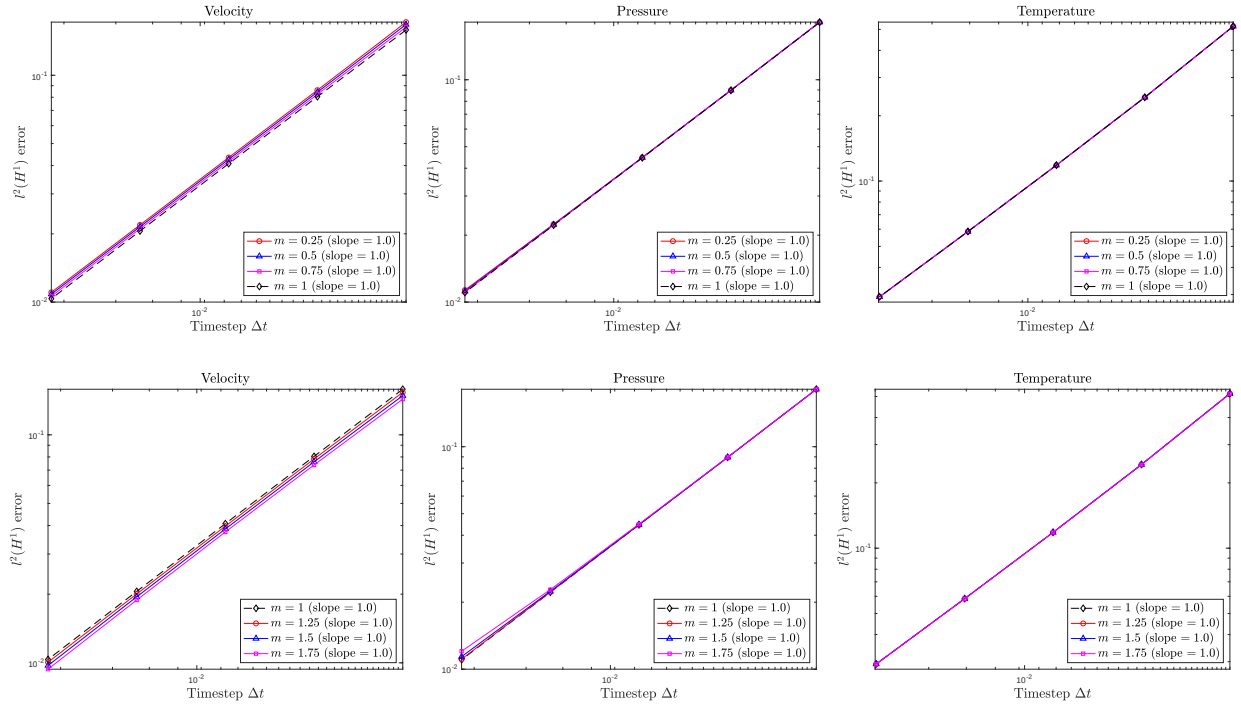

Figure 2: Convergence results using the $l^2(H^1)$-error for the velocity $\boldsymbol{u}$ (first column), pressure p (second column) and temperature Θ (third column) obtained for the accuracy example using $m \leq 1$ (first row) and $m \geq 1$ (second row).

It is evident that the analytical solutions (52) are manufactured to be polynomials in space with the same degree as the finite element polynomial basis. This would drastically reduce the spatial errors and enable a better assessment of the behavior of time errors which are the prime interest of the current work. For this example, the convergence rates are calculated using errors between the analytical and numerical solutions computed using the following discrete norms

$$\|\boldsymbol{e}\|_{l^2(X)} = \left(\Delta t \sum_{n=0}^{N} \|e^n\|_X\right)^{1/2}, \qquad \|\boldsymbol{e}\|_{l^\infty(X)} = \sup_{n=0,\ldots,N} \|\boldsymbol{e}^n\|_X,$$

where X is assumed to be as $\boldsymbol{L}^2(\Omega)$ or $\boldsymbol{H}^1(\Omega)$ for the velocity solution, and as $L^2(\Omega)$ or $H^1(\Omega)$ for temperature and pressure solutions. We use different timesteps evaluated by $\Delta t = \dfrac{0.1}{2^k}$ $(k = 1, \ldots, 5)$ and the obtained results are presented at the final time $t = 0.5$ using a structured finite element mesh with $20 \times 20 \times 20$ elements.

In Figure 1 we present the computed errors for the velocity $\boldsymbol{u}$, the pressure p and temperature Θ in the selected $l^2\left(0, T_f; L^2(\Omega)\right)$ norm for both cases of shear-thinning fluids ($m < 1$) and shear-thickening fluids ($m > 1$). Those errors computed using the $l^2\left(0, T_f; H^1(\Omega)\right)$ norm are displayed in Figure 2. It is clear that for this test example, the convergence plots demonstrate that the $\boldsymbol{L}^2$-error and $\boldsymbol{H}^1$-error for the velocity solution and the L^2-error and H^1-error for the temperature solution are of full first-order as predicted by the established error estimates. In addition, the convergence rates achieved for the pressure solution in both $l^2\left(0, T_f; L^2(\Omega)\right)$ and $l^2\left(0, T_f; H^1(\Omega)\right)$ norms reveal a higher order than the theoretical $1/2$-order estimated in Theorem 2. This behavior can be attributed to the fact that the established error estimates of the pressure solution are sub-optimal and they can be further improved. For the considered test example, it is also clear that the obtained error plots for both cases of shear-thinning and shear-thickening fluids maintain the same trend which is also consistent with the error estimates proved in the present study for the proposed fractional time-stepping method.

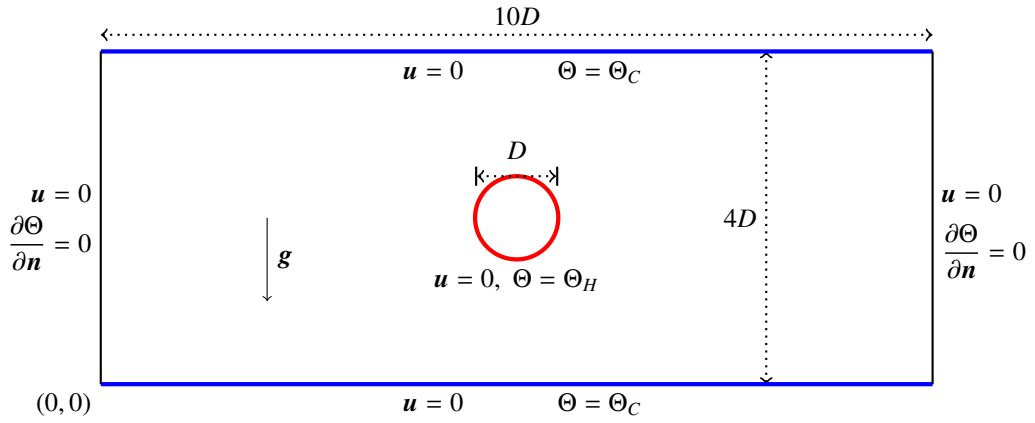

Figure 3: Domain configuration along with the boundary conditions used for the problem of thermal flow past a circular cylinder.

5.2. *Thermal flow past a circular cylinder*

In this test example we consider the problem of an incompressible shear-thinning fluid confined in a horizontal rectangular domain containing a hot circular cylinder in the middle and undergoing a natural convection phenomenon due to a temperature difference between the cylinder surface and the domain upper and lower walls. Here, we solve the two-dimensional equations (4) in a rectangular domain of length $10D$ and height $4D$, with $D = 0.1\ m$ represents the diameter of the cylinder located in the centre of the domain as shown in Figure 3. The boundary conditions used for the temperature and flow velocity are also illustrated in this figure. Here, the cylinder is maintained heated at a constant hot temperature $\Theta_H = 30°C$ while the upper and lower walls of the domain are maintained at a cold temperature $\Theta_C = 20°C$, and the two vertical walls are thermally insulated. No-slip boundary condition $\boldsymbol{u} = \boldsymbol{0}$ is applied on all boundaries of the computational domain. It is well known that when the temperature difference $\Theta_H - \Theta_C$ is large enough, a convection flow phenomena is triggered for which the high-temperature fluid rises up around the cylinder under the effect of the buoyancy force. Thus, using the well-established Boussinesq approximation, the source terms in (4) are given by

$$\alpha\, \boldsymbol{f}(\Theta) = \beta \boldsymbol{g}\,(\Theta - \Theta_C)\,, \qquad \boldsymbol{g} = \left(0, 9.8\ m/s^2\right)^\top, \qquad g = 0,$$

where β is the coefficient of thermal expansion and $\boldsymbol{g}$ represents the gravitational force. In all the simulations reported in this section, the physical parameters are set to be shear-rate and temperature-dependent according to the the following laws

$$\nu(\Theta, \boldsymbol{Du}) = \nu_\infty + (\gamma(\Theta) - \nu_\infty)\left(1 + \beta_0^2\, \|\boldsymbol{Du}\|^2_{\mathbb{R}^{2\times 2}}\right)^{\frac{m-1}{2}}, \qquad \gamma(\Theta) = \gamma_0\left(1 + e^{-\gamma_1 \Theta}\right), \qquad \lambda(\Theta) = \kappa\,(1 + \epsilon\Theta)\,,$$

with

$$\gamma_0 = 5 \times 10^{-4}, \qquad \gamma_1 = 1, \qquad \beta_0 = \sqrt{2}, \qquad \nu_\infty = 2.5 \times 10^{-4}, \qquad \kappa = 2.2 \times 10^{-5}, \qquad \epsilon = 0.3.$$

As in most natural convection problems, the Rayleigh number Ra and the Prandtl number Pr associated with this example are defined as

$$Ra = \frac{\beta \|\boldsymbol{g}\|(\Theta_h - \Theta_c)D^3}{\kappa\gamma_0}, \qquad Pr = \frac{\gamma_0}{\kappa}.$$

In our computations for this example, we use an unstructured triangular mesh of 29018 mixed elements with 14509 pressure nodes, and 57491 velocity and temperature nodes. This mesh offers a compromise between accuracy and efficiency in the proposed fractional time-stepping method. The timestep Δt is fixed to 0.05 s and steady-state numerical results are presented for the Prandtl number $Pr = 0.71$ and two different Rayleigh numbers namely, $Ra = 10^3$ and $Ra = 10^4$.

Figure 4 depicts the temperature distributions and the streamlines along with the velocity magnitudes obtained using the selected values of the power index $m = 0.2$, 0.4, 0.6, 0.8 and 1 at the Rayleigh number $Ra = 10^3$. Those

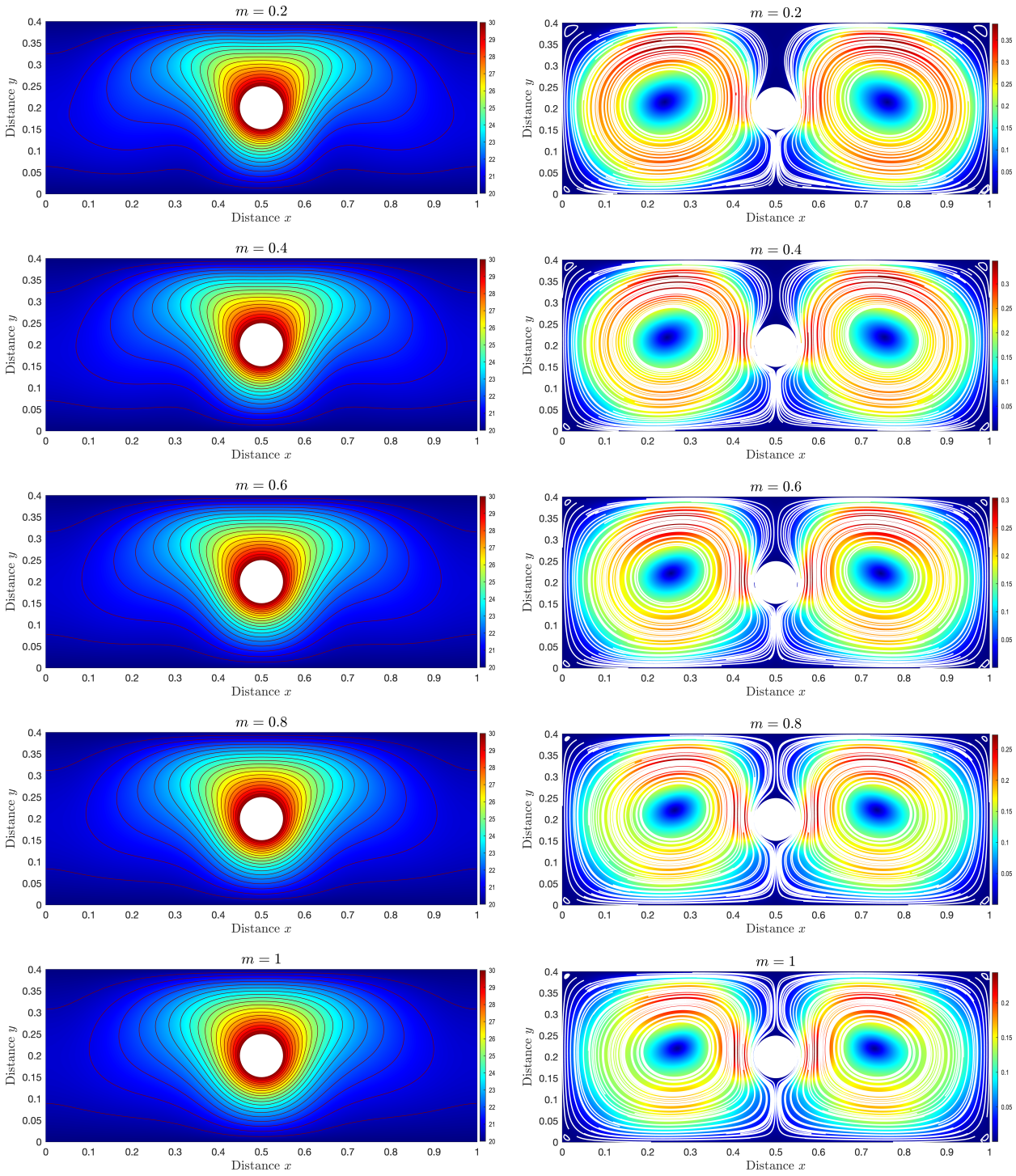

Figure 4: Temperature distribution along with isotherms (first column) and velocity magnitude along with streamlines (second column) for the problem of thermal flow past a circular cylinder using $Ra = 10^3$ and different values of the power index. From top to bottom $m = 0.2$, 0.4, 0.6, 0.8 and 1.

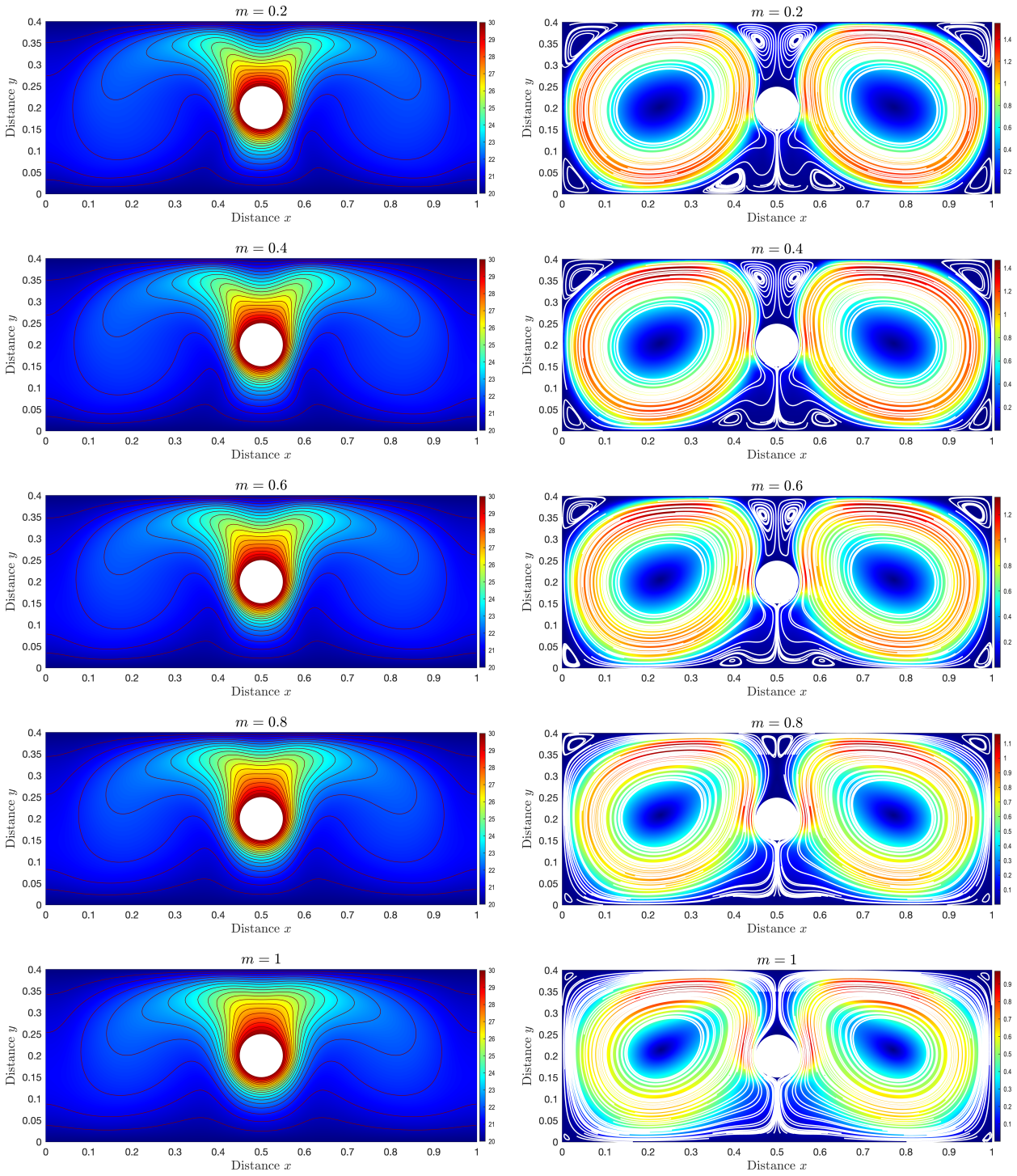

Figure 5: Same as Figure 4 but using $Ra = 10^4$.

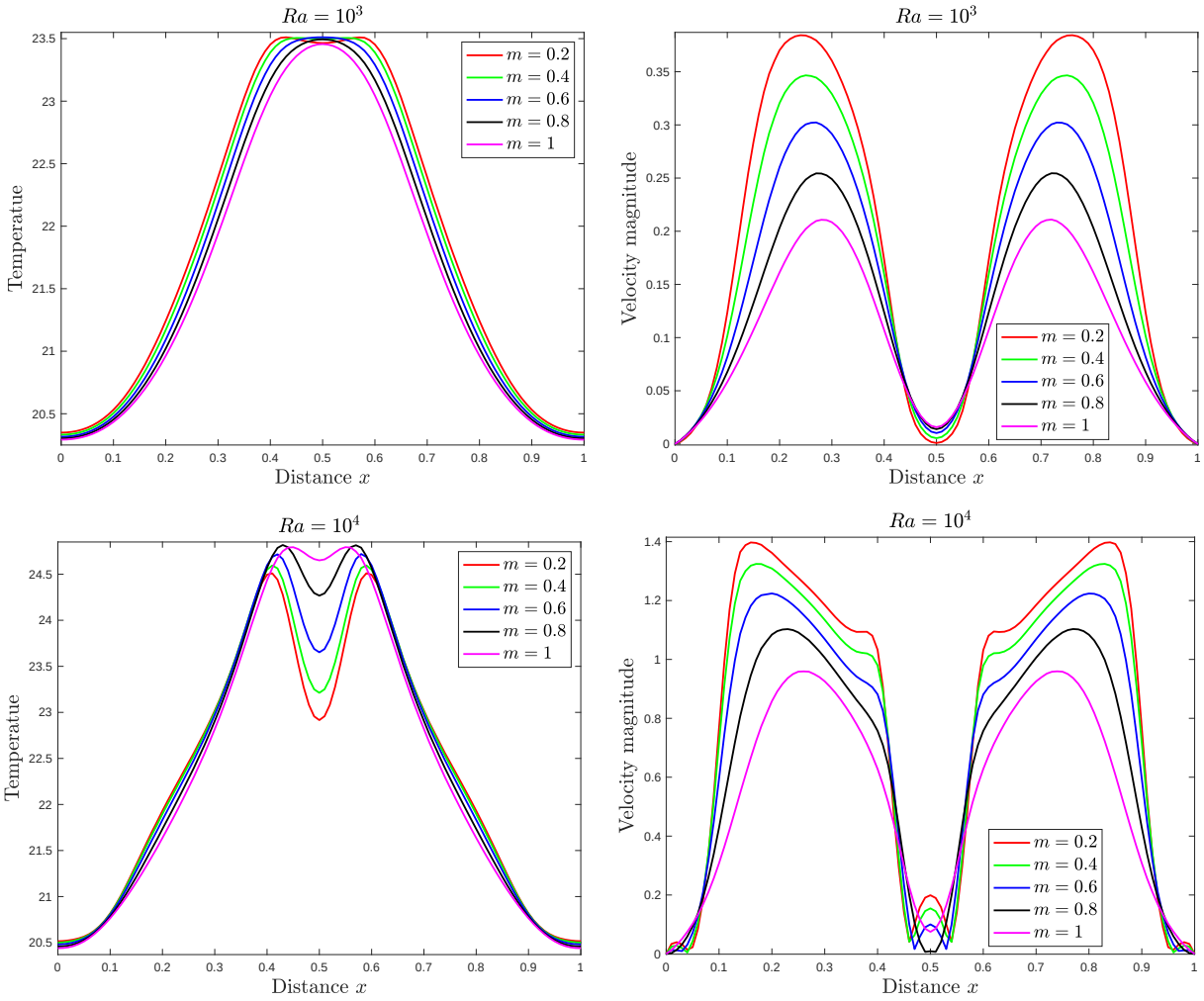

Figure 6: Horizontal cross-sections at $y = 3.5D$ of the temperature (first column) and velocity magnitude (second column) for the problem of thermal flow past a circular cylinder using $Ra = 10^3$ (first row) and $Ra = 10^4$ (second row) with different values of the power index.

results obtained using the Rayleigh number $Ra = 10^4$ are presented in Figure 5. For the considered natural convection regimes, we clearly see the formation of two symmetrical main recirculation zones rotating in opposite directions to each other in addition to four smaller vortices at the corners. The temperature distribution on the other side, indicates that the heat transfer through natural convection has already taken place at the selected Pr and Ra numbers for all values of the power index m. As the Rayleigh number increases, the main flow recirculations intensify and collide with obvious distortions near the upper half (respectively, lower half) of the thermal source where two vertical (respectively, horizontal) and symmetrical vortices appear in the shear-thinning case $m < 1$ (starting from $m = 0.8$), separating the main ones. Moreover, the vortices at the corner become elongated with more intensity and growth in the upper ones. This is mainly due to the fact that the natural convection turns stronger for large Rayleigh numbers and it tends to perturb the flow behavior vertically since it is acting against the gravity. This also explains the concentration of temperature contours in the upper zone near the hot cylinder where convective heat transfer is more important. For this test example, it can be clearly seen that the complicated flow and heat features are well captured by the proposed fractional time-stepping method.

The influence of shear-thinning on the flow structures and heat features is also noticeable from the results included in Figure 4 and Figure 5. Here, as the power index m decreases, strong shear-thinning takes place and it weakens the

Table 1: Coordinates of centers of the main recirculations (scaled by the diameter D) for the problem of thermal flow past a circular cylinder using $Ra = 10^3$ and $Ra = 10^4$ with different values of the power index m.

Ra	Vortex	$m = 1$	$m = 0.8$	$m = 0.6$	$m = 0.4$	$m = 0.2$
10^3	Left	(2.715, 2.194)	(2.633, 2.206)	(2.544, 2.219)	(2.449, 2.194)	(2.403, 2.156)
	Right	(7.329, 2.182)	(7.347, 2.224)	(7.453, 2.216)	(7.555, 2.202)	(7.607, 2.150)
10^4	Left	(2.293, 2.149)	(2.302, 2.100)	(2.255, 2.057)	(2.308, 2.046)	(2.260, 2.002)
	Right	(7.703, 2.148)	(7.692, 2.087)	(7.726, 2.051)	(7.726, 2.051)	(7.760, 2.016)

Table 2: Averaged Nusselt number for the problem of thermal flow past a circular cylinder using $Ra = 10^3$ and $Ra = 10^4$ with different values of power index m.

Ra	$m = 1$	$m = 0.8$	$m = 0.6$	$m = 0.4$	$m = 0.2$
10^3	35.6237	36.4612	37.456	38.4998	39.489
10^4	52.311	55.7395	58.3358	59.9684	60.8314

viscosity in the high shear-stress regions near the cylinder and the domain walls. Thus, with the viscous effects that tend to dissipate energy being less intense, the momentum becomes dominant and is transferred from the cylinder region, where the velocity is greater due to the natural convection, to the surroundings. This is clearly seen from the velocity distribution in the case with $m = 0.2$, where the recirculation velocity almost keeps its highest magnitude compared to the case with $m = 0.8$, where the recirculation velocity is higher near the cylinder and much weaker far from it. Moreover, as shear-thinning effects increase, the corner vortices (especially the upper ones) become enlarged and squeeze the two main recirculation regions inward. Additionally, the small pairs of symmetrical vortices above and under the cylinder become larger and push as well the main ones horizontally, which transforms them to a rather more oval shape for $m = 0.2$ compared to greater values of m. This displacement of the main recirculation zones is clearly shown in Table 1, where coordinates of their corresponding centers, scaled by the cylinder diameter, are listed. We can see that as m drops towards $m = 0.2$, the horizontal displacement is more important at $Ra = 10^3$, while at $Ra = 10^4$, the vertical displacement prevails. The former is due to the forthcoming two vortices above the cylinder where the main ones move away horizontally as preparations for their appearance. As pointed out before, the latter is due to the important growth of the upper corner vortices. This also confirms that the proposed fractional time-stepping method is very attractive since the computed flow solutions remain stable and accurate for the thermal convection in non-Newtonian fluids.

To further illustrate the influence of the power index m on the flow and heat patterns, Figure 6 presents horizontal cross-sectional profiles of the velocity magnitude and temperature above the cylinder at $y = 3.5D$. From the first glance, we can see a perfect symmetry with respect to the vertical centerline for all values of m at both selected Rayleigh numbers. On the other hand, the noticeable effect of decreasing the power index m on the velocity and temperature solutions is also detected in these results. As the power index m goes far from the Newtonian regime, the velocity intensifies significantly above the cylinder due to the greater convection process in this region, especially at higher Rayleigh numbers. For the same reasons, the temperature profile undergoes important changes localized near the cylinder, which also explains the structure of temperature contours of Figure 5, which shows more curvature and more concentration in the upper region as m decreases. This emphasizes the fact that stronger shear-thinning features induce stronger convective heat transfer, and consequently, a complex flow behavior takes place. To further demonstrate this impact, Table 2 summarizes the variations of the averaged Nusselt number as a function of the power index m. Notice that the averaged Nusselt number quantifies the ratio of heat transfer by convection to heat transfer

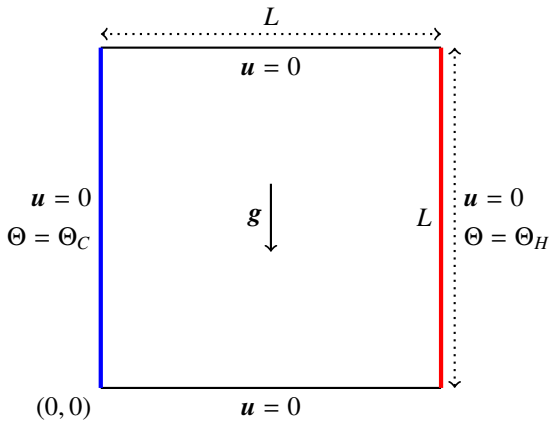

Figure 7: Domain configuration along with the boundary conditions used for the problem of natural convection in a square enclosure with differentially heated side walls.

by conduction, and it is computed along the surface of the cylinder as

$$Nu = \oint_{\partial\mathcal{D}} \frac{\partial\Theta}{\partial \boldsymbol{n}} ds,$$

where $\boldsymbol{n}$ is the outward normal vector on the cylinder surface $\partial\mathcal{D}$. As it can be seen from the Table 2, the Nusselt number increases monotonically with growing shear-thinning features such that more increase is expected for higher Rayleigh numbers. This means that more natural convection is occurring at low values of m and consequently more complex behavior for the fluid flow as explained before. Moreover, under the conditions of the present test example, the influence of m on the averaged Nusselt number in the conditions of the present test, seems overall to be weak at low Rayleigh numbers and intensifies as the later grows. These observations are qualitatively in good agreement with the published results on the flow behavior of shear-thinning fluids under natural convection, see for instance [44] and the references therein.

5.3. Natural convection in a square enclosure with differentially heated side walls

Our final test example consists of applying the proposed viscosity-splitting method to a natural convection problem of power-law fluids in a square enclosure with differentially heated side walls investigated in [54] among others. Here, we solve the equations (4) in a two-dimensional squared cavity of length L differentially heated from the sides and filled of a fluid equipped with the power-law model for the shear-rate-viscosity relationship given by

$$\nu(\boldsymbol{Du}) = \nu_p \left(2\,\|\boldsymbol{Du}\|^2_{\mathbb{R}^{2\times 2}}\right)^{\frac{m-1}{2}}, \tag{53}$$

where ν_p is the so-called consistency coefficient of the power-law model. The flow is subject to no-slip boundary conditions on the cavity walls. The right wall is maintained hot at constant temperature Θ_H and the left one is kept at cold temperature Θ_C with a difference $\Delta\Theta = \Theta_H - \Theta_C = 10\ K$, while the horizontal boundaries are insulated. Detailed description of the computational domain and boundary conditions for this problem are sketched in Figure 7. It should be stressed that these fluid flows are known to be highly driven by two non-dimensional coefficients namely, the Rayleigh number Ra and the Prandtl number Pr which are defined here as

$$Ra = \frac{g\,\alpha\,\Delta\Theta\,L^{2m+1}}{\nu_p\,(\lambda_p)^m} \qquad \text{and} \qquad Pr = \nu_p(\lambda_p)^{m-2}\,L^{2-2m},$$

where λ_p is the thermal diffusivity coefficient assumed to be constant in our simulations. Hence, the Rayleigh number quantifies the relative strength of natural convection induced by the buoyancy force to the dissipative effects due to

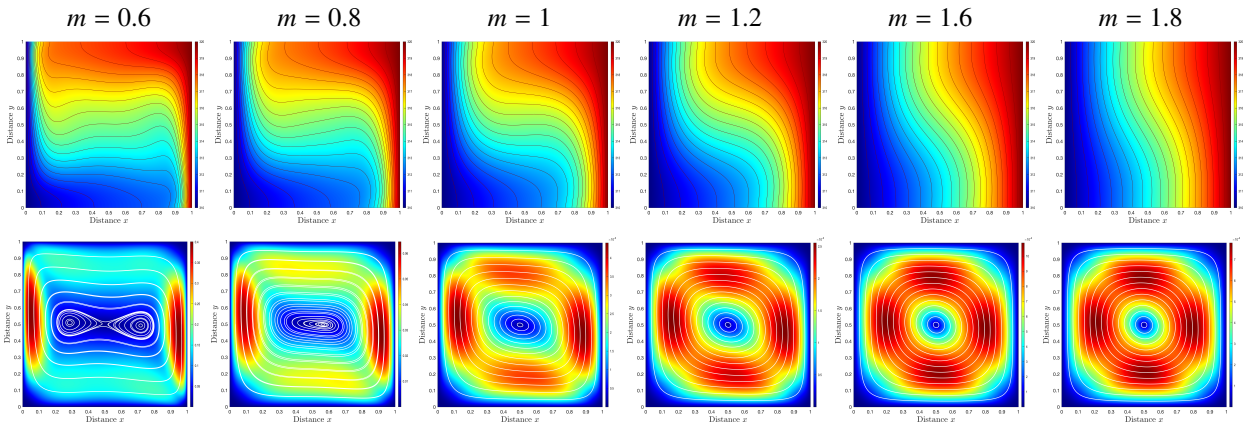

Figure 8: Temperature distribution along with isotherms (first row) and velocity magnitude along with streamlines (second row) for the problem of natural convection in a square enclosure with differentially heated side walls using $Pr = 100$ and different values of the power index. From left to right $m = 0.6$, 0.8, 1, 1.2, 1.6 and 1.8.

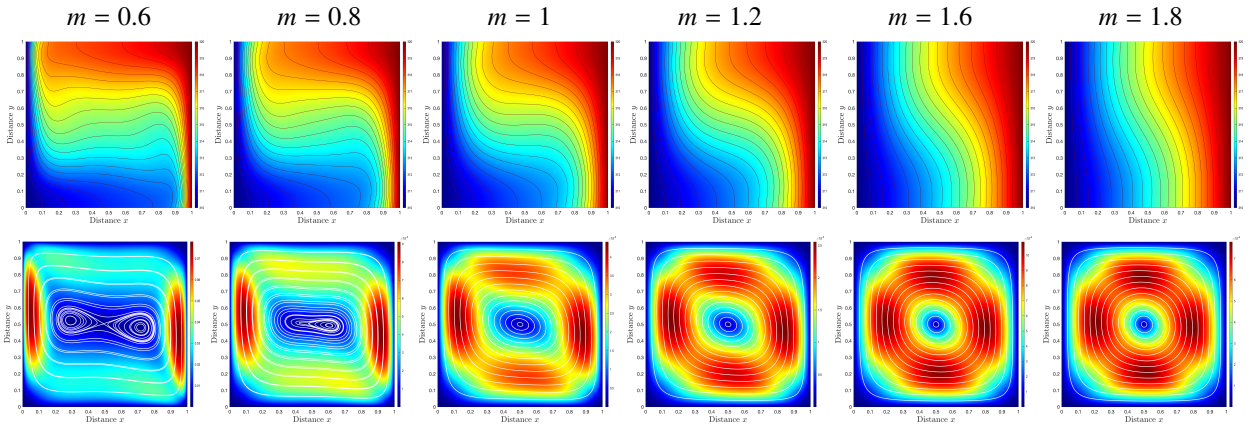

Figure 9: Same as Figure 8 but using $Pr = 1000$.

viscosity and thermal diffusion, whereas the Prandtl number indicates the relative importance between the momentum transport and the thermal transport. For this problem, we use the same parameters as in [54] such as the Rayleigh number $Ra = 10^4$, the Prandtl number $Pr = 100$ and 1000, and the power index $m = 0.6$, 0.8, 1, 1.2, 1.4, 1.6 and 1.8 which covers a wide range of Non-Newtonian fluids including shear-thinning fluids ($m < 1$) and shear-thickening fluids ($m > 1$). For the mixed finite element discretization, an unstructured triangular mesh of 11412 elements with 5707 pressure nodes, and 22573 velocity and temperature nodes is used in our computations.

In Figure 8 we present the temperature distributions along with isotherms and the streamlines along with the velocity magnitudes obtained using the selected values of the power index $m = 0.6$, 0.8, 1, 1.2, 1.6 and 1.8 for the Prandtl number $Pr = 100$. Those results obtained using the Prandtl number $Pr = 1000$ are illustrated in Figure 9. It is clear from these results that the flow field of power-law fluids at the considered Rayleigh and Prandtl numbers generates a recirculation zone centered in the middle of the domain and rotating in the counterclockwise direction. This recirculation zone is more circular at higher values of the power-index $m = 1.6$ and 1.8 but becomes distorted in the anti-diagonal direction as m tends to the Newtonian case ($m = 1$). In the shear-thinning case ($m < 1$), the corresponding central zone becomes stretched horizontally until it splits into two smaller symmetrical vortices at $m = 0.6$. Notice that the distortion indicates the dominance of the convective transport occurring vertically where the hot fluid from the right wall is rising up due to the buoyancy then travelling to the colder left wall where it is cooled and

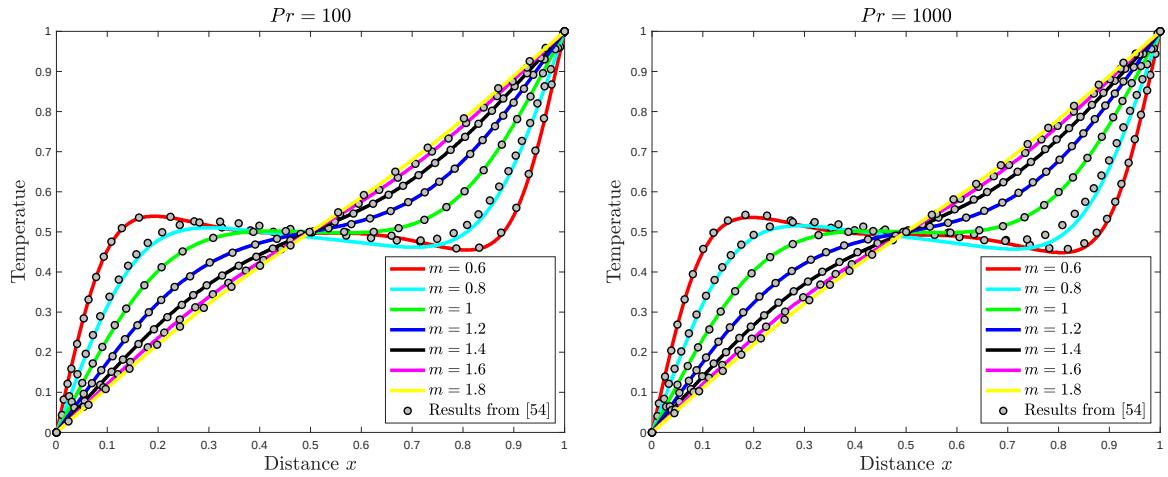

Figure 10: Horizontal cross-sections at $y = 0.5$ of the temperature for the problem of natural convection in a square enclosure with differentially heated side walls using $Pr = 100$ (left) and $Pr = 1000$ (right) with different values of the power index.

Table 3: Mean Nusselt number for the problem of natural convection in a square enclosure with differentially heated side walls using $Pr = 100$ and $Pr = 1000$ with different values of power index m.

Pr	$m = 1.8$	$m = 1.6$	$m = 1.4$	$m = 1.2$	$m = 1$	$m = 0.8$	$m = 0.6$
100	1.09784	1.18186	1.35520	1.68755	2.27492	3.48246	5.76528
1000	1.09786	1.18184	1.35519	1.68757	2.27491	3.51869	5.86870

pushed down by gravity. For shear-thickening fluids ($m > 1$), increasing the power-index m strengthens the viscosity (especially near the walls) and by-product natural convection motion is dumped by the dissipative viscous effects that tends to stabilize the flow field. Therefore, we observe more regular and symmetrical velocity distributions with weaker magnitudes as m grows larger than unity. On the other hand, strong shear-thinning effects tend to weaken the viscous forces letting the convection motion to prevail and consequently a more agitated flow takes place. Moreover, the influence of the power-index on this flow problem is also clearly noticeable from the temperature distributions in Figure 8 and Figure 9 where the isotherms have sharper deviations at low values of $m < 1$ suggesting greater heat transfer by natural convection. The latter form of heat transfer is enfeebled by increasing $m > 1$ giving the dominance to conductive heat transport which explains the isotherms becoming less distorted as we reach $m = 1.8$. These results are almost identical for both considered Prandtl numbers $Pr = 100$ and 1000 indicating that at $Ra = 10^4$ the flow is weakly influenced by the Prandtl number. These results also agree well with those reported in [54] for the same flow parameters.

To further demonstrate the previous observations more closely, we display in Figure 10 horizontal cross-sections of the dimensionless temperature at the centerline for different values of the power-index m. For comparison purposes, we also include results from [54] in these plots. It is obvious from Figure 10 that the temperature distribution is more nonlinear at lower power-index values of $m < 1$ and tends to become linear as we move towards the shear-thickening case and closer to $m = 1.8$. This confirms the previous conclusions that due to high shear-thickening effects, the heat is mainly transported by conduction, while convective heat transport overcomes in the shear-thinning case. Comparing the results obtained using our viscosity-splitting method to those published in [54], it shows almost a perfect agreement which illustrates the efficiency of the proposed method not only for shear-thinning fluids but also for shear-thickening fluids at high Prandtl numbers. To quantify these effects, we also calculate the mean Nusselt number defined by

$$\overline{Nu} = \frac{1}{\Theta_H - \Theta_C} \oint_{\partial\mathcal{L}} \frac{\partial\Theta}{\partial \boldsymbol{n}} ds,$$

where $\boldsymbol{n}$ is the outward normal vector on the right wall $\partial\mathcal{L}$. The results obtained for the mean Nusselt number are summarized in Table 3 for the two considered Prandtl numbers and the selected values of the power-index m. It is evident that $\overline{Nu}$ increases as the power-index decreases with significant growth in the shear-thinning case, which in turn emphasizes the importance of heat transfer by convection occuring at low values of m as observed before. Moreover, the temperature profiles and the mean Nusselt numbers at $Pr = 100$ are almost the same as those obtained at $Pr = 1000$ which also confirms the weak influence of the Prandtl number on this flow problem at the present flow conditions.

6. Conclusions

In this paper, we presented a fractional-step method for the numerical solution of unsteady thermal convection in incompressible non-Newtonian fluids whose viscosity is temperature and shear rate-dependent according to a generic law with temperature-dependent thermal conductivity. The method employs viscosity-splitting techniques that efficiently remove any numerical boundary layer by maintaining the full original boundary conditions. It also allows the temperature to be transported by a non-divergence-free velocity, which is an unusual feature in most existing methods in the literature. We conducted a rigorous error analysis for all the solutions and established first-order accuracy for both velocity and temperature solutions and $1/2$-order accuracy for the pressure solution in their appropriate norms. To assess the computational performance of the fractional-step method, numerical results obtained for a three-dimensional example with the manufactured exact solution and for the benchmark of a thermal flow past a circular cylinder are presented. The method is also applied for solving a natural convection problem of power-law fluids in a square enclosure with differentially heated side walls. The results obtained for these examples confirm the convergence, accuracy and applicability of the proposed time fractional-step method for solving thermal convection in non-Newtonian fluids. Future work will focus on establishing error estimates for the fully discrete problems. Extension of this analysis to thermal non-Newtonian fluids with more generalized constitutive laws will also be considered for future work.

Declaration of competing interest

The authors declare that they have no known competing financial interests or personal relationships that could have appeared to influence the work reported in this paper.

Data availability

The data that support the findings of this study are available from the corresponding author upon reasonable request.

Acknowledgment

The authors would like to thank anonymous referees for giving very helpful comments and suggestions that have greatly improved this paper.

Appendix A.

Denote by G_1 the mapping defined, for all fixed $\boldsymbol{s} \in \mathbb{R}^{d\times d}$ by

$$\begin{aligned} G_1 : \mathbb{R} &\longrightarrow \mathbb{R} \\ t &\longrightarrow \nu_\infty + (\gamma(t) - \nu_\infty)\left(1 + \beta_0^2 \|\boldsymbol{s}\|^2_{\mathbb{R}^{d\times d}}\right)^{\dfrac{m-1}{2}}, \end{aligned}$$

with the same parameters m, ν_∞, γ and β_0 as in (7). Hence, the derivative of G_1 is given by

$$G_1^{'}(t) = \left(1 + \beta_0^2 \|\boldsymbol{s}\|^2_{\mathbb{R}^{d\times d}}\right)^{\dfrac{m-1}{2}} \gamma^{'}(t), \qquad \forall \boldsymbol{s} \in \mathbb{R}^{d\times d}.$$

Since $m \leq 1$ and thanks to (8), it is easy to verify that

$$\|G_1^{'}\|_\infty \leq C,$$

where the constant C is independent of $\boldsymbol{s}$. Denote by G_2 the mapping defined, for all fixed $t \in \mathbb{R}$, by

$$\begin{aligned} G_2 : \mathbb{R}^{d\times d} &\longrightarrow \mathbb{R} \\ s &\longrightarrow \nu_\infty + (\gamma(t) - \nu_\infty)\left(1 + \beta_0^2 \|\boldsymbol{s}\|^2_{\mathbb{R}^{d\times d}}\right)^{\dfrac{m-1}{2}}, \end{aligned}$$

with the same parametersm, ν_∞, γ and β_0 as in (7). Thus, its differential is given, for all fixed $t \in \mathbb{R}$, by

$$dG_2(\mathbf{s}) : \mathbf{h} \longrightarrow (m-1))\beta_0^2(\gamma(t) - \nu_\infty)\left(1 + \beta_0^2 \|\mathbf{s}\|^2_{\mathbb{R}^{d\times d}}\right)^{\alpha-1} \langle \mathbf{s}, \mathbf{h}\rangle, \qquad \forall\ \mathbf{h} \in \mathbb{R}^{d\times d}.$$

It is readily verified that

$$\sup_{\mathbf{s}\in\mathbb{R}^{d\times d}, \mathbf{s}\neq 0} \frac{\|dG_2(\mathbf{s})\|}{\|\mathbf{s}\|_{\mathbb{R}^{d\times d}}} \leq C_\nu,$$

where

$$C_\nu = |m-1|\beta_0\,(\nu_1 - \nu_\infty)\left(\frac{2(1-\alpha)}{1-2\alpha}\right)^{\alpha-1} \frac{1}{\sqrt{1-2\alpha}}.$$

Thanks to the mean-value theorem (see for instance [47]) we can write

$$\begin{aligned} |\nu(t_1, \boldsymbol{s}_1) - \nu(t_2, \boldsymbol{s}_2)| &\leq |\nu(t_1, \boldsymbol{s}_1) - \nu(t_2, \boldsymbol{s}_1)| + |\nu(t_2, \boldsymbol{s}_1) - \nu(t_2, \boldsymbol{s}_2)|, \\ &\leq C|t_1 - t_2| + C_\nu \|\boldsymbol{s}_1 - \boldsymbol{s}_2\|_{\mathbb{R}^{d\times d}}. \end{aligned} \tag{A.1}$$

Next, we can bound the last two terms of (34) as follows

$$\begin{aligned} I_1 &= -4\Delta t \int_\Omega \left(\nu(\Theta_{\mathcal{R}}(t_{n+1}), \boldsymbol{Du}(t_{n+1})) - \nu(\Theta^n_{\mathcal{R}}, \boldsymbol{Du}^n)\right) \boldsymbol{Du}(t_{n+1}) : \boldsymbol{D\bar{e}}_u^{n+1}\, d\boldsymbol{x} \\ &\leq 4C_u\Delta t \left(\int_\Omega |\nu(\Theta_{\mathcal{R}}(t_{n+1}), \boldsymbol{Du}(t_{n+1})) - \nu(\Theta^n_{\mathcal{R}}, \boldsymbol{Du}^n)|^2\, d\boldsymbol{x}\right)^{1/2} \|\boldsymbol{D\bar{e}}_u^{n+1}\|, \text{ (Cauchy-Schwarz's inequality and (27))} \\ &\overset{By(A.1)}{\leq} 4C_u\Delta t \left(\int_\Omega (C|\Theta(t_{n+1}) - \Theta^n| + C_\nu \|\boldsymbol{Du}(t_{n+1}) - \boldsymbol{Du}^n\|_{\mathbb{R}^{d\times d}})^2\, d\boldsymbol{x}\right)^{1/2} \|\boldsymbol{D\bar{e}}_u^{n+1}\|, \\ &\leq C\Delta t \left(\|\Theta(t_{n+1}) - \Theta(t_n)\| + \|e^n_\Theta\| + \|\boldsymbol{Du}(t_{n+1}) - \boldsymbol{Du}(t_n)\|\right) \|\boldsymbol{D\bar{e}}_u^{n+1}\| + 4\sqrt{2}C_u\, C_\nu \Delta t \|\boldsymbol{De}_u^n\|\, \|\boldsymbol{D\bar{e}}_u^{n+1}\|, \\ &\leq C(\Delta t)^2 \int_{t_n}^{t_{n+1}} \|\partial_t\Theta\|^2 dt + C(\Delta t)^2 \int_{t_n}^{t_{n+1}} |\partial_t \boldsymbol{u}|_1^2 dt + C\Delta t \|e^n_\Theta\|^2 + 2\frac{C_r \nu_\infty \Delta t}{J} |\bar{\boldsymbol{e}}_u^{n+1}|_1^2 + \frac{8JC_u^2\, C_\nu^2}{\nu_\infty C_r} \Delta t |\boldsymbol{e}_u^n|_1^2. \end{aligned}$$

Similarly,

$$
\begin{aligned}
I_2 &= 4\Delta t \int_\Omega \Big(\nu(\overline{\Theta}_{\mathcal{R}}^{n+1}, \boldsymbol{Du}^n) - \nu(\Theta_{\mathcal{R}}^n, \boldsymbol{Du}^n)\Big)\boldsymbol{Du}(t_{n+1}) \colon \boldsymbol{De}_u^{n+1}\, d\boldsymbol{x}, \\
&\leq 4C_u\Delta t\left(\int_\Omega \left(C|\overline{\Theta}^{n+1} - \Theta^n|\right)^2\right)^{1/2} \|\boldsymbol{De}_u^{n+1}\|, \text{ (Cauchy-Schwarz's inequality and (27))} \\
&\leq C\Delta t\left(\|\Theta(t_{n+1}) - \Theta(t_n)\| + \|\overline{e}_\Theta^{n+1} - e_\Theta^n\|\right)\|\boldsymbol{De}_u^{n+1}\|, \\
&\leq C(\Delta t)^2 \int_{t_n}^{t_{n+1}} \|\partial_t\Theta\|^2 dt + C\Delta t\|\overline{e}_\Theta^{n+1} - e_\Theta^n\|^2 + (2\nu_\infty - \nu_1)C_r\Delta t|\boldsymbol{e}_u^{n+1}|_1^2.
\end{aligned}
$$

References

[1] R. A. Adams. *Sobolev Spaces*. Academic Press New York, 1975.

[2] A. Bejan. *Convection heat transfer*. John wiley & sons, 2013.

[3] J. Bell, P. Colella, and H. Glaz. A second-order projection method for the incompressible Navier-Stokes equations. *J. of Comp. Physics*, 85(2):257–283, 1989.

[4] J.-M. Bernard. Density results in Sobolev spaces whose elements vanish on a part of the boundary. *Chinese Annals of Mathematics. Series B*, 32(6):823–846, 2011.

[5] C. Bernardi, B. Métivet, and B. Pernaud-Thomas. Couplage des équations de Navier-Stokes et de la chaleur: le modèle et son approximation par éléments finis. *RAIRO Modélisation Mathématique et Analyse Numérique*, 29(7):871–921, 1995.

[6] J. Blasco and R. Codina. Error estimates for an operator-splitting method for incompressible flows. *Appl. Numer. Math.*, 51(1):1–17, 2004.

[7] J. Blasco, R. Codina, and A. Huerta. A fractional-step method for the incompressible Navier-Stokes equations related to a predictor-multicorrector algorithm. *Internat. J. Numer. Methods Fluids*, 28(10):1391–1419, 1998.

[8] F. Boyer and P. Fabrie. *Mathematical Tools for the Study of the Incompressible Navier-Stokes Equations and Related Models*, volume 183 of *Applied Mathematical Sciences*. Springer, New York, 2013.

[9] I. Bugarin and T. Oliveira. Droplet motion in confined natural convection flows. *International Journal of Heat and Mass Transfer*, 173:121249, 2021.

[10] P. J. Carreau. Rheological Equations from Molecular Network Theories. *Transactions of The Society of Rheology*, 16(1):99–127, 03 1972.

[11] H. Choi, H. Choi, and J. Yoo. A fractional four-step finite element formulation of the unsteady incompressible Navier-Stokes equations using supg and linear equal-order element methods. *Computer Methods in Applied Mechanics and Engineering*, 143(3-4):333–348, 1997.

[12] H. Choi and P. Moin. Effects of the computational time step on numerical solutions of turbulent flow. *Journal of Computational Physics*, 113(1):1–4, 1994.

[13] A. Chorin. Numerical solution of the Navier–Stokes equations. *Math. Comp.*, 22:745–762, 1968.

[14] P. Constantin. C. foias, Navier-Stokes equations. *Chicago Lectures in Math. Series, Univ. of Chicago Press*, 1988.

[15] J. Deteix, A. Jendoubi, and D. Yakoubi. A Coupled Prediction Scheme for Solving the Navier–Stokes and Convection-Diffusion Equations. *SIAM Journal on Numerical Analysis*, 52(5):2415–2439, 2014.

[16] J. Deteix and D. Yakoubi. Improving the pressure accuracy in a projection scheme for incompressible fluids with variable viscosity. *Applied Mathematics Letters*, 79:111–117, 2018.

[17] J. Deteix and D. Yakoubi. Shear rate projection schemes for non-Newtonian fluids. *Computer Methods in Applied Mechanics and Engineering*, 354:620–636, 2019.

[18] Y. I. Dimitrienko and S. Li. Numerical simulation of mhd natural convection heat transfer in a square cavity filled with carreau fluids under magnetic fields in different directions. *Computational and Applied Mathematics*, 39(4):252, 2020.

[19] K. A. Dittko, M. Kirkpatrick, and S. Armfield. Natural convection in a sidewall heated cube using an immersed boundary method. *ANZIAM Journal*, 52:C535–C548, 2010.

[20] M. El-Amrani, A. Obbadi, M. Seaid, and D. Yakoubi. Error estimates for a viscosity-splitting scheme in time applied to non-Newtonian fluid flows. *Computer Methods in Applied Mechanics and Engineering*, 419:116639, 2024.

[21] J. H. Ferziger and M. Perić. *Computational methods for fluid dynamics*. Springer, 2002.

[22] V. Girault and P.-A. Raviart. *Finite Element Methods for the Navier-Stokes Equations*, volume 5 of *Springer Series in Computational Mathematics*. Springer-Verlag, Berlin, 1986.

[23] R. Glowinski, T.-W. Pan, and J. Périaux. A fictitious domain method for external incompressible viscous flow modeled by Navier-Stokes equations. *Computer Methods in Applied Mechanics and Engineering*, 112:133–148, 1994.

[24] K. Goda. A multistep technique with implicit difference schemes for calculating two- or three-dimensional cavity flows. *Journal of Computational Physics*, 30(1):76–95, 1979.

[25] J. Guermond and J. Shen. On the error estimates for the rotational pressure-correction projection methods. *Mathematics of Computation*, 73(248):1719–1737, 2004.

[26] J. L. Guermond, P. Minev, and J. Shen. Error Analysis of Pressure-Correction Schemes for the Time-Dependent Stokes Equations with Open Boundary Conditions. *SIAM Journal on Numerical Analysis*, 43(1):239–258, 2006.

[27] F. Guillén-González and M. Redondo-Neble. New error estimates for a viscosity-splitting scheme in time for the three-dimensional Navier-Stokes equations. *IMA J. Numer. Anal.*, 31(2):556–579, 2011.

[28] J. G. Heywood and R. Rannacher. Finite-Element Approximation of the Nonstationary Navier–Stokes Problem. Part IV: Error Analysis for Second-Order Time Discretization. *SIAM Journal on Numerical Analysis*, 27(2):353–384, 1990.

[29] Y. Hou, W. Yan, and J. Hou. A fractional-step DG-FE method for the time-dependent generalized Boussinesq equations. *Communications in Nonlinear Science and Numerical Simulation*, 116:106884, 2023.
[30] R. Huilgol and G. Kefayati. Natural convection problem in a bingham fluid using the operator-splitting method. *Journal of Non-Newtonian Fluid Mechanics*, 220:22–32, 2015.
[31] F. Irgens. *Rheology and Non-Newtonian Fluids*. Springer International Publishing, Cham, 2014.
[32] D. D. Joseph. On the stability of the Boussinesq equations. *Arch. Ration. Mech. Anal.*, 29:32–57, 1965.
[33] G. Karniadakis, M. Israeli, and S. Orszag. High-order splitting methods for the incompressible Navier–Stokes equations. *Journal of Computational Physics*, 97(2):414–443, 1991.
[34] J. Kim and P. Moin. Application of a fractional-step method to incompressible Navier–Stokes equations. *Journal of Computational Physics*, 59(2):308–323, 1985.
[35] S. Kopecz, M. Krebs, A. Meister, and O. Wünsch. A fast numerical approach for the simulation of highly viscous non-isothermal non-Newtonian fluids. *Zeitschrift für angewandte Mathematik und Physik*, 61:673–684, 2010.
[36] S.-J. Liang, Y.-J. Jan, and C.-A. Huang. A quasi-implicit time-advancing scheme for 3-d Rayleigh-bénard convection. *Numerical Heat Transfer, Part B: Fundamentals*, 63(5):371–394, 2013.
[37] J.-L. Lions and E. Magenes. *Problèmes Aux Limites Non Homogènes et Applications*, volume 1. Dunod, 1968.
[38] D. Lo, D. Young, and Y. Lin. Finite-element analysis of 3-d viscous flow and mixed-convection problems by the projection method. *Numerical Heat Transfer, Part A: Applications*, 48(4):339–358, 2005.
[39] Y. Lung-an. Viscosity-splitting scheme for the Navier-Stokes equations. *Numerical Methods for Partial Differential Equations*, 7(4):317–338, 1991.
[40] P. Nithiarasu. A unified fractional step method for compressible and incompressible flows, heat transfer and incompressible solid mechanics. *International Journal of Numerical Methods for Heat & Fluid Flow*, 18(2):111–130, Mar. 2008.
[41] S. A. Orszag, M. Israeli, and M. O. Deville. Boundary conditions for incompressible flows. *Journal of Scientific Computing*, 1(1):75–111, 1986.
[42] D. R. Pacheco, R. Schussnig, and T.-P. Fries. An efficient split-step framework for non-Newtonian incompressible flow problems with consistent pressure boundary conditions. *Computer Methods in Applied Mechanics and Engineering*, 382:113888, 2021.
[43] L. Plasman, J. Deteix, and D. Yakoubi. A projection scheme for Navier-Stokes with variable viscosity and natural boundary condition. *International Journal for Numerical Methods in Fluids*, 92(12):1845–1865, 2020.
[44] A. Prhashanna and R. Chhabra. Laminar natural convection from a horizontal cylinder in power-law fluids. *Industrial & engineering chemistry research*, 50(4):2424–2440, 2011.
[45] Y. Qian and T. Zhang. On error estimates of the projection method for the time-dependent natural convection problem: first order scheme. *Computers & Mathematics with Applications*, 72(5):1444–1465, 2016.
[46] Y. Qian and T. Zhang. The second order projection method in time for the time-dependent natural convection problem. *Applications of Mathematics*, 61(3):299–315, 2016.
[47] W. Rudin. *Principles of mathematical analysis*. 1953.
[48] D. Shang. *Free convection film flows and heat transfer*. Springer, 2006.
[49] J. Shen. On error estimates of projection methods for Navier-Stokes equations: First-order schemes. *SIAM Journal on Numerical Analysis*, 29(1):57–77, 1992.
[50] J. Shen. On error estimates of the projection methods for the Navier-Stokes equations: Second-order schemes. *Mathematics of Computation*, 65(215):1039–1066, July 1996.
[51] R. Temam. Sur l'approximation de la solution des équations de Navier-Stokes par la méthode des pas fractionnaires (I). *Archive for Rational Mechanics and Analysis*, 32(2):135–153, Jan. 1969.
[52] R. Temam. Remark on the pressure boundary condition for the projection method. *Theoretical and Computational Fluid Dynamics*, 3(3):181–184, 1991.
[53] L. J. P. Timmermans, P. D. Minev, and F. N. V. D. Vosse. An Approximate Projection Scheme for Incompressible Flow Using Spectral Elements. *International Journal for Numerical Methods in Fluids*, 22(7):673–688, 1996.
[54] O. Turan, A. Sachdeva, N. Chakraborty, and R. J. Poole. Laminar natural convection of power-law fluids in a square enclosure with differentially heated side walls subjected to constant temperatures. *Journal of Non-Newtonian Fluid Mechanics*, 166(17-18):1049–1063, 2011.
[55] J. van Kan. A second-order accurate pressure-correction scheme for viscous incompressible flow. *Society for Industrial and Applied Mathematics. Journal on Scientific and Statistical Computing*, 7(3):870–891, 1986.
[56] W. Wang, J. Wu, and X. Feng. A novel pressure-correction projection finite element method for incompressible natural convection problem with variable density. *Numerical Heat Transfer, Part A: Applications*, 74(2):1001–1017, 2018.
[57] H. Welhezi, N. Ben-Cheikh, and B. Ben-Beya. Numerical analysis of natural convection between a heated cube and its spherical enclosure. *International Journal of Thermal Sciences*, 150:105828, 2020.
[58] J. Wu, X. Feng, and F. Liu. Pressure-correction projection fem for time-dependent natural convection problem. *Communications in Computational Physics*, 21(4):1090–1117, 2017.
[59] D. Yakoubi. Enhancing the viscosity-splitting method to solve the time-dependent Navier–Stokes equations. *Communications in Nonlinear Science and Numerical Simulation*, 123:107264, 2023.
[60] Y.-B. Yang, B.-C. Huang, and Y.-L. Jiang. Error estimates of an operator-splitting finite element method for the time-dependent natural convection problem. *Numerical Methods for Partial Differential Equations*, 39(3):2202–2226, 2023.